Master's thesis

NTNU
Norwegian University of Science and Technology
Faculty of Engineering
Department of Mechanical and Industrial Engineering

Asim Mansoor Jilani

Consequence Analysis of Hydrogen Explosion during Transportation

Master's thesis in Reliability, Availability, Maintainability, and Safety
Supervisor: Nicola Paltrinieri
Co-supervisor: Cecilia Haskins, Federico Ustolin
June 2021

NTNU
Norwegian University of
Science and Technology

Asim Mansoor Jilani

Consequence Analysis of Hydrogen Explosion during Transportation

Master's thesis in Reliability, Availability, Maintainability, and Safety
Supervisor: Nicola Paltrinieri
Co-supervisor: Cecilia Haskins, Federico Ustolin
June 2021

Norwegian University of Science and Technology
Faculty of Engineering
Department of Mechanical and Industrial Engineering

Abstract

New carbon emissions targets for 2050 are peaking interest in the market for hydrogen as an alternative energy source. MCE, a supplier of road transportation solutions, requested the support of their planning and decision-making regarding options for the transport of compressed hydrogen gas.

The thesis work is the continuation of the specialization project of fall semester 2020 directed towards the domain of the risk analysis of the storage equipment under transport in particular for compressed hydrogen tanks. The thesis presents the risk analysis of the potential consequences based on multiple scenarios regarding the transportation of the compressed hydrogen tank and the driver's cabin safety. The major focus has been on the consequence modeling of rupture of the hydrogen tank using computational fluid dynamics (CFD) modeling to simulate and evaluate the impact of the blast wave generated on the driver's cabin and the surrounding environment in terms of pressure and temperature profiles. The results support the analysis of measures required to prevent and minimize the effects of the consequences. However, additional work remains toward establishing clear guidelines for safeguarding the transport of hydrogen gas in terms of regulations such as the European Agreement concerning the International Carriage of Dangerous Goods by Road (ADR).

Sammendrag

Nye karbonutslippsmål for 2050 er i etterpurt interesse for markedet for hydrogen som en alternativ energikilde. MCE, en leverandør av løsninger for veitransport, ba om støtte til planlegging og beslutningstaking angående muligheter for transport av komprimert hydrogengass.

Oppgavearbeidet er en videreføring av spesialiseringsprosjektet høstsemesteret 2020 rettet mot domenet for risikoanalysen av lagringsutstyret under transport, spesielt for komprimerte hydrogentanker. Oppgaven presenterer risikoanalysen av de potensielle konsekvensene basert på flere scenarier angående transport av komprimert hydrogentank og førerhusets sikkerhet. Hovedfokus har vært på konsekvensmodellering av brudd i hydrogentanken ved bruk av numerisk fluiddynamikk modellering for å simulere og evaluere virkningen av eksplosjonsbølgen generert på førerhuset og det omkringliggende miljøet når det gjelder trykk og temperaturprofiler. Resultatene støtter analysen av tiltak som er nødvendige for å forhindre og minimere konsekvensene. Imidlertid gjenstår det ytterligere arbeid med å etablere klare retningslinjer for å sikre transport av hydrogengass i form av forskrifter som den Europeisk avtale om internasjonal transport av farlig gods på vei.

Preface

The thesis is part of the two-year International master's degree program in Reliability, Availability, Maintainability, and Safety (RAMS) Engineering at the Norwegian University of Science and Engineering (NTNU). The thesis is carried out in collaboration with the company, MCE AS during the spring semester of 2021.

Acknowledgment

I would like to extend gratitude to the supervisor, Associate Professor Nicola Paltrinieri for his constant mentoring and guidance throughout the project. In addition, the support and constant feedback of our co-supervisor Associate Professor Cecilia Haskins has played a major role in completing this project and meeting the expectations of the company MCE. I want to thank the second co-supervisor Ph.D. candidate, Federico Ustolin for being of great help with his broad knowledge of hydrogen and modeling works.

We would also like to thank the CEO of MCE, Eldar Tranøy, for his support and interest throughout the project.

Table of Contents

List of Figures

List of Tables

Acronyms

ADR	European Agreement concerning the International Carriage of Dangerous Goods by Road
ARAMIS	Accidental Risk Assessment Methodology for Industries
CcH2	Cryo-Compressed Hydrogen
CCS	Carbon Capture and Storage
CFD	Computational Fluid Dynamics
CGH2	Compressed Gas Hydrogen
LH2	Liquified or liquid hydrogen
LOC	Loss of containment
LPI	Loss of physical integrity
MIMAH	Methodology for the identification of major accident hazards
MLI	Multi-layer insulation
NTP	Normal temperature and pressure; (293.15K, 101.325kPa)
SRM	Steam reforming of methane
VCE	Vapor cloud explosion

1 Introduction

To contribute to the carbon reduction policy goals of the current energy systems, the introduction of different types of alternative fuels and energy sources shows a significant role and possibility of long-lasting outcomes to stimulate these goals. With the emergence of the Hydrogen Economy, employing hydrogen indicates the potential to replace conventional fuels in the future.

Hydrogen is an energy carrier and must be produced from an energy source. Hydrogen can be considered a low or zero-emission carrier if the methods of production utilize non-fossil fuels such as biomass, organic matter, water electrolysis, etc. (Ustolin, Paltrinieri et al. 2020). The production of hydrogen from fossil fuels subsequently requires carbon separation techniques to be considered a clean source of energy.

Hydrogen storage is the viable approach for extensive use in the transport and maritime sector and safety analysis must be assessed (Galassi, Baraldi et al. 2012). According to (Pant and Gupta 2009), it must be compressed to increase its energy density and to improve its storage and transport capacity. The challenges for using hydrogen as an energy carrier vary with the state of the hydrogen being used for storage and transportation. The choice of the state of hydrogen is subject to several factors such as storage capacities, demand volumes, and transport distances (Yang and Ogden 2007). Compressed hydrogen can be transported in gas tanks on trucks, ships, and trains. Pipeline transport is a viable transporting medium for large distances.

MCE is a production company, with modern production facilities located in Etne municipality. MCE has broad expertise in dealing with engineering materials for the construction of large vehicles' bodywork, production, installation of steel structures, and is also a distributor of industrial gases. The company plans to contribute to the clean energy market and intends to add the transportation of hydrogen to its industrial gas distribution business.

In autumn semester 2020, a specialization report on the state of the art of hydrogen technology was presented in collaboration with MCE AS. In the report, a detailed analysis of hydrogen as an energy carrier was presented differentiating the use of hydrogen in different forms and its respective storage technologies. On the basis of the analysis and the company's expertise, the motivation towards the transportation of compressed gaseous hydrogen (CGH2) was shown by the MCE company. This led to the detailed study of the CGH2 tank risk analysis on Norwegian roads. In this thesis, the risk analysis part has been covered using modeling of severe consequences involved during the transportation of CGH2 tanks on a truck.

The thesis work is based on the risk analysis of the consequences involved during the transportation of the CGH2. Based on the study conducted in the specialization project, a detailed risk analysis is conducted on the possible consequences involved during the transportation of CGH2 tanks. The study is backed up by the detailed consequence modeling of the rupture suggesting safety measures to prevent the consequence.

From this study, it is expected that the company will have the risk analysis conducted in line with the European Agreement concerning the International Carriage of Dangerous

Goods by Road (ADR) on the truck design and operations. First, the analysis can be used to make potential changes in the design of trucks. Second, it introduces additional safety barriers to make the system more safe and reliable. Third, the risk assessments are in alignment with the ADR regulations, especially for Norwegian roads.

1.1 Motivation and Objectives

The motivation of the thesis is linked with the growing interest of the Norwegian authorities toward the Paris agreement 2050 to reduce carbon emissions. Hydrogen as an alternative energy carrier and a replacement for conventional fossil fuels looks promising. The master's thesis has been carried out in collaboration with the Norwegian company MCE AS. Based on the study conducted in the specialization report on the state of the art of hydrogen storage options and transportation, the company plans to select the CGH2 solution. The main objectives of the analysis are as follows.

- Identify and analyze the potentially critical consequences involved during the road transportation of CGH2.
- Use the experimental and theoretical data available in the literature to model the consequences of a rupture of a CGH2 tank, and identify the usable data and limitations of the model to be simulated for the company. The consequence analysis will be able to identify the risk imposed on the human.
- Identify the current knowledge gaps in the safety regulations that govern transportation on Norwegian roads related to the transport of CGH2.

The results from the literature and model developed should provide a holistic view on the possible risks involved in road transportation of CGH2 during operations. MCE can then decide on significant design modifications to their current transportation product lines and develop their safety guidelines in advance of lagging European policy.

1.2 Thesis scope and limitations

The thesis scope is the risk analysis of the consequences involved during the transportation of the CGH2. The study consists of detailed consequence modeling of the CGH2 tank rupture showing the effects of a blast wave generated on the surroundings. The limitation expected from the consequence simulation will neglect the contribution of combustion which can affect the estimation of blast wave strength.

1.3 Outline

The rest of the thesis follows the following structure. Chapter 2 reflects the background of hydrogen technology and the types of storage involved in CGH2 transportation. Chapter 3 focuses on the methodology used for the risk analysis and consequence modeling. Chapter 4 is the main section of the study consisting of the simulation results of the tank rupture consequence. Chapter 5 discusses the significance of the results achieved and safety measures in terms of design to prevent the impact of such consequences. Chapter 6 concludes the study objectives, identifies the limitations and further research directions.

2 Background

In this chapter, the background of hydrogen as an element, its current production techniques, properties, and a comparison to conventional fuel is discussed briefly to have an understanding of the aesthetics of hydrogen. Consequently, the next section will be followed up with the current hydrogen storage and transportation technologies. Thus, gradually developing a bridge between the background presented and the motives of the thesis. The background is backed up by the risk analysis concepts and regulations concerning the storage and transport of dangerous fuels.

2.1 Hydrogen Properties

Hydrogen is the lightest element in nature, and at atmospheric conditions, it is a diatomic gas with a very low density of 0.0838 kg/m^3 at normal temperature and pressure (NTP) (Salvi and Subramanian 2015). Hydrogen gas is colorless, odorless, non-corrosive, and non-toxic. Hydrogen gas has high diffusivity, buoyancy, faster flame velocity, and hotter flame temperatures in comparison with fossil fuels (Pant and Gupta 2009). Hydrogen gas is classified as flammables, requiring relatively low energy for ignition, i.e. 0.02 mJ (Pant and Gupta 2009). Hydrogen has a high gravimetric energy density (140 MJ/kg vs 48.6 MJ/kg) in comparison to gasoline that makes it a promising candidate as an energy carrier (Pant and Gupta 2009).

Hydrogen is one of the most promising candidates for replacing fossil fuels in the future. Hydrogen has high energy content per unit of mass (140 MJ/kg) in comparison with gasoline (48.6 MJ/kg) (Pant and Gupta 2009).

Table 1: Properties of hydrogen in comparison with Gasoline(Das 1990, White, Steeper et al. 2006, Pant and Gupta 2009)

Properties	Hydrogen	Gasoline
Density (kg/m^3)	0.08987	730
Flame Velocity (m/s)	1.85	0.37-0.43
Minimum Ignition energy (mJ)	0.02	0.24
Autoignition temperature in air (K)	858	550
The heat of Combustion (MJ/kg$_{air}$)	3.37	2.83
Flammability Limits (Φ)	0.1 - 7.1	0.7 - 4

Table 1 shows the comparison of some selective properties of hydrogen in comparison to gasoline. The properties like high heat of combustion, high flammability limits, and low minimum ignition energy for hydrogen gas in a controlled environment make it a favorable choice as fuel. For hydrogen just like any other fuel to combust, an oxidizing source like air and a source of ignition are necessary for its combustion. The combustible nature raises

a lot of questions and clarification in terms of safety and risk when dealing with hydrogen at high pressures in different applications such as transportation.

2.2 Production of hydrogen

The most appealing characteristic of hydrogen as an energy carrier is the production of hydrogen from the multiple available energy sources. The production has a large impact on the carbon footprints depending on the source used to generate hydrogen such as fossil fuels or renewables (Gandía, Arzamendi et al. 2013). For hydrogen to be clean and emissions-free, clean production methods have to be identified (Probstein and Hicks 2006).

Based on the source of energy used and the method of production, hydrogen is usually categorized as: grey, blue, and green. Grey hydrogen utilizes fossil fuels through a series of thermochemical processes. The most common, mature, and least expensive method to produce hydrogen is steam reforming of methane (SRM) which accounts for 95% of the production in the world (Dickel 2020). SRM process adds a significant amount of CO_2 per unit of hydrogen produced when methane is the hydrogen source. Steam reforming using non-fossil energy sources like nuclear and solar energy is not only energy-efficient but has significant capacity to mitigate carbon emissions (Kumar 2015). Grey hydrogen is low cast but has low social acceptance due to the carbon emissions. The SRM will continue to be the current producer's most fundamental choice for hydrogen production, as long as the prices of natural gas remain moderate (Gandía, Arzamendi et al. 2013).

Blue hydrogen is not inherently free from carbon, but the CO2 is separated by means of Carbon Capture and Storage (CCS) and CCS technology is costly (Wang, Li et al. 2018). Blue hydrogen is cheaper than green hydrogen (Noussan, Raimondi et al. 2021). Blue hydrogen is a cost-effective and practicable technology that can be used in industry (Van Cappellen, Croezen et al. 2018).

Green hydrogen is the most socially desirable hydrogen, produced using clean energy sources, such as wind and solar. The electric energy generated by the renewables can feed the electrolysis process to produce hydrogen from water. As this process is clean there are no requirements to employ the CCS technique. However, if the electricity supplied to the electrolyzer is generated by means of fossil fuels, the produced hydrogen cannot be considered as green. Electrolyzer commercial units are capable of producing approximately 600 t of hydrogen per year with a power rating of 3.5 MW. It is argued that blue hydrogen is a much more feasible approach than green hydrogen based on cost-benefit analysis. Finally, the large-scale production of green hydrogen is not economically viable (Dickel 2020).

The energy sources and technologies adopted to produce hydrogen using renewables and non-renewable energy sources are reported in table 2. Non-renewable energy sources contribute over 96% of the total worldwide hydrogen production out of which, 48% is achieved by SRM, 30% from hydrocarbons fractions, 18% from gasification of coal. Only 4% of hydrogen is produced through water electrolysis which is considered a clean and renewable process (Armaroli and Balzani 2011).

Norway has a high untapped potential for wind power and a very high fraction of hydroelectric power (Ulleberg and Hancke 2020). For this reason, Norway seems an ideal candidate for producing zero-emissions hydrogen utilizing electrolysis.

Table 2: Hydrogen production sources and technologies (Gandía, Arzamendi et al. 2013)

Primary Energy	Secondary energy	Conversion Technologies	Hydrogen production type
Natural gas & Hydrocarbons	Heat	Reforming	Nonrenewable Hydrogen
	-	Partial oxidation	
	Electricity	Water Electrolysis	
Coal	Heat	Gasification	
	Electricity	Water Electrolysis	
Nuclear	Heat	Thermochemical cycles	
	Electricity	Water Electrolysis	
Biomass	-	Gasification & Reforming	Renewable Hydrogen
	-	Anaerobic fermentation	
Solar	Heat	Water Thermolysis	
		Photo electrolysis	
		Photocatalytic water splitting	
		Water Electrolysis	
	Electricity	Water Thermolysis	
		Photo electrolysis	
		Photocatalytic water splitting	
Wind	Electricity	Water Electrolysis	
		Water Thermolysis	
		Photo electrolysis	
		Photocatalytic water splitting	

2.3 Storage and Transportation Technologies

Hydrogen as a fuel can be stored either as a compressed gas or in a liquid phase. There are still several barriers that must be considered when storing or transporting hydrogen. For instance, the lack of hydrogen infrastructure and the hydrogen low density are two limitations when stored (Varin and Wronski 2013).

The current ways to store hydrogen can be categorized by the temperature and pressure operating values. For instance, CGH2 tanks operate at high pressures (e.g. 70 MPa) and ambient temperatures. Cryo-compressed hydrogen (CcH2) tanks can bear pressures ranging 25 – 35 MPa and temperatures between 150 K and 273 K (Ahluwalia, Hua et al. 2010). Lastly, liquid hydrogen vessels operate at low pressure (0.6 MPa) and temperatures near the hydrogen boiling point (Stetson, McWhorter et al. 2016).

To transport hydrogen effectively it is required to be stored at a higher volumetric density. Usually, increasing density requires significant cost and energy. As previously mentioned, the hydrogen density can be improved by compressing or liquefying it. In this thesis, the focus will be on CGH2 using high-pressure storage tanks.

2.3.1 Compressed Hydrogen

The compression of hydrogen at high pressures (35 to 70 MPa) makes it possible for its transportation and onboard storage in the automobile using standard types of tanks. One of the key advantages of adopting CGH2 is the possibility to quickly refill the storage tanks.

Approximately 3 to 5 minutes are required to refill hydrogen-powered vehicles (Stetson, McWhorter et al. 2016). When dealing with CGH2 the safety of these storages is always of concern. The safety part of CGH2 storage is discussed in the next chapter.

Commercial tube trailers are usually filled at central hydrogen production plants where compressors are used to increase the hydrogen pressure. The CGH2 trucks are usually known as large semi-trucks carrying tubes to transport and store CGH2. These trailers consist of 12 to 20 steel cylinders mounted on the trailer bed. The cylinders are usually grouped in bundles and are filled at filling stations and are delivered to the final consumer by replacing them with empty cylinders with filled ones (Gerboni 2016). A typical truck consists of nine CGH2 tubes, each with a volume of 91.8 ft^3 (2.60m^3) (Chen 2010).

The gas pressures are normally around 160 bar (can go up to 400 bar at special certifications) and the amount of CGH2 carried is around 300kg (Yang and Ogden 2007). Tube trailers could be used to supply small quantity demands and over short distances, for example, less than 200 miles (320 km) (Simbeck and Chang 2002) (Drive 2017).

For storage of CGH2 the following standard types of cylinders are commercially available (Stetson, McWhorter et al. 2016):

- Type I - all metal cylinders
- Type II - all metal with hoop wrapped composite cylinders
- Type III - fully wrapped composite cylinders with metallic liners
- Type IV - fully wrapped composite cylinders with no-load bearing non-metallic liners

2.3.1.1 Type I tank

Type I tanks are all made of steel and the metallic construction makes these tanks heavy. It is the most common type of tank used in industries. The advantage of using type I tanks is that they are cheaper to fabricate and appropriate for static applications. On the other hand, the excessive weight makes it unfavorable to use for mobile applications such as transportation. The hydrogen mass is only 1% to 2% of the tank mass (Stetson, McWhorter et al. 2016). This makes it less favorable for compressed hydrogen storage.

2.3.1.2 Type II

Type II tanks also possess full metallic construction, but metal liners are much thinner, and the hoop wrapped with carbon fiber provides reinforcement for the tank. The construction makes these types of tanks lighter than type I. Type II is more suited for applications having low cost in comparison to storage pressures and weights. Similar to tank I, the mass of the tank can accommodate 1 to 2% of hydrogen storage with respect to tank mass (Stetson, McWhorter et al. 2016). As Type I, these tanks are impractical in transportation where weight and volumes are important factors.

2.3.1.3 Type III

Type III consists of a thin and light metal line that is overwrapped with carbon composites. The design and construction of Type III tanks are more expensive than type I and II. Type III are lighter, can fill hydrogen at higher pressures, and consequently offer higher capacities at least four times that of Type I and II of the same tank size (Stetson, McWhorter et al. 2016).

2.3.1.4 Type IV

Type IV is constructed predominantly from carbon composite materials and a polymer liner. This type of tank is the lightest one, making it the most suitable for portable applications as well as and the most expensive. With this design, the capacities to store compressed hydrogen are increased up to 4.4% of hydrogen with respect to the mass of the tank (McWhorter and Ordaz 2013). This is higher than Type I and II tanks' capacities at higher pressures. However, type IV has few drawbacks. It is more resistant to damage, and polymer lining is not an impermeable barrier. So, there is a higher chance of loss of containment in case of leakage compared with the other types.

2.3.2 Cryogenic storage - Liquid hydrogen

As mentioned earlier, the low hydrogen density makes it inefficient to transport and store it. However, the hydrogen density can be increased by liquification. Hydrogen is converted into liquid through the liquification process. The liquification process consists of a series of compressions and heat exchanges which are usually carried out at the production facilities. The liquification process energy requirement and costs are higher than for compression process, but the cryogenic liquid trucks can carry at least ten times larger mass almost 4000 kg of hydrogen (Yang and Ogden 2007) (Simbeck and Chang 2002). Liquid hydrogen (LH2) storages are relatively cheaper than CGH2 storages when dealing with capital cost per liter handled (Simbeck and Chang 2002). LH2 is used to deliver higher quantities over long distances within the range of 600 miles (966 km) as compared to CGH2 (Simbeck and Chang 2002) (Drive 2017).

LH2 can be transported using cryogenic truck tankers of capacities ranging from 30 to 60m^3 (Sherif, Zeytinoglu et al. 1997). The truck capacity is up to 4000kg (Simbeck and Chang 2002) and pressures around 0.6 to 1.0 MPa (Yang and Ogden 2007).

The use of well-insulated cryogenic storage vessels enables the prevention of boil-off and increases the hydrogen storage duration by reducing the venting losses. The design promotes larger capacities and compact sizes. Tank structures consist of an evacuated double-walled container, and different types of insulation can be adopted. Multi-layer insulation (MLI) and perlite (silica powder) are the most common insulations for LH2 tanks. This design reduces thermal conductions and evaporation losses (Stetson, McWhorter et al. 2016).

LH2 trucks consist of a single hydrogen tank mounted on the trailer. The truck usually fills at central plant and supplies to required stations which can be one or multiple in one trip (Yang and Ogden 2007).

2.4 Potential hydrogen applications

The development of hydrogen as a major alternative fuel source depends on several factors at the time of analysis. The recession in the petroleum industry during the COVID-19 pandemic has further shifted the attention of major energy producers towards renewable energies and hydrogen. The 2014 crude oil prices recession resulted in shifting the medium of transport to hydrogen in the fast-going passenger boats along the Norwegian coast (Renkel and Lümmen 2018). Many experts believe that the substantial effect of the evolution of the hydrogen economy will be seen around 2040 and the development in this sector is not rapid (Kim, Boo et al. 2014). However, the emergence of hydrogen systems will be evident in the long term and highly depends on the demand and supply flow of this economy (Kim, Boo et al. 2014). The possibility lies in the pathway from the producers to consumers as shown in figure 1.

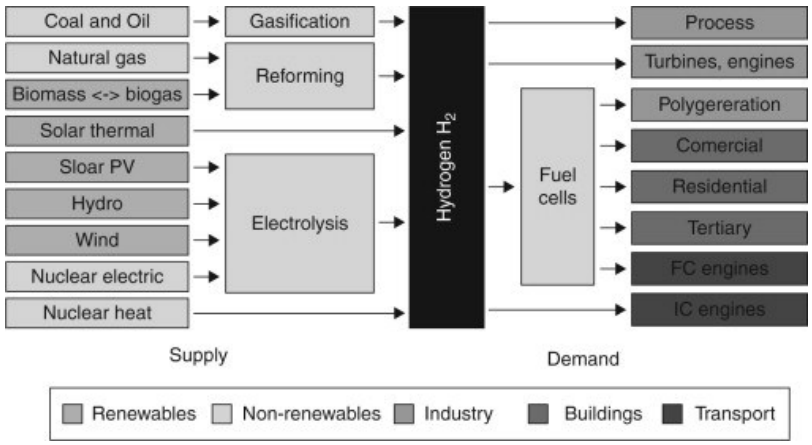

Figure 1: Hydrogen sources and applications (Stygar and Brylewski 2013)

There is a surge in the interest of the Norwegian government and private sector in producing hydrogen. The Norwegian clean energy cluster shows a promising hydrogen facility at Haugalandet by 2024. Besides, in Kvinnehard, Norsk Hydro's electrolysis plant is expected to come into operation by the end of 2020. There are several hydrogen producers in Norway. Yara and Equinor together produce 180000 tons per annum out of the total national production of Hydrogen (Damman, Sandberg et al. 2020). Other notable producers and distributors are Nippon gases and Ineos.

The commercial areas for hydrogen as fuel in Norway are the Maritime sector (Damman, Sandberg et al. 2020), but the usage in road transport and process industries is also emerging. In Kvinnherad, Sunnhordaland Kraftlag (power producer) and Gasnor (gas producer) signed an agreement to manufacture a liquid hydrogen plant (Damman, Sandberg et al. 2020). As a major potential customer, a new tender is released for starting a high-speed passenger vessel between Bergen and Rosendal requiring approximately 512 kg of hydrogen per week (Damman, Sandberg et al. 2020). In January 2020, ASKO started using the world's first hydrogen-powered trucks, with a range of 500km, and initially operated in Trondheim (Norwegian Ministry of Petroleum and Energy 2020). The list of potential consumers increases as the government promotes and invests in this technology.

2.5 Hydrogen Safety

The emergence of hydrogen systems brings challenges one of the most important is safety and handling. The limited commercial exposure and defined regulations make it difficult to define or present the safety of hydrogen handling effectively. Hydrogen characteristics are not only attractive but if not handled safely the consequences could be severe. Hydrogen being the lightest element, odorless, and colorless gas makes it difficult to detect in case of a leak from its storage equipment. Hydrogen mixes with air and forms a flammable mixture that might burn or explode in presence of an ignition source. Hydrogen is categorized as flammable gas and has low minimum ignition energy of 0.02 mJ (Pant and Gupta 2009).

When the behavior of hydrogen is compared with one of the other conventional hydrocarbons (e.g. methane, gasoline), its flame is non-luminous, the flammability range is extremely wide, and its diffusive nature disperses the flammable cloud swiftly (Wurster 2016). These characteristics impose a big challenge to handle it safely. Table 3 compares the hydrogen properties with other two conventional hydrocarbons: methane and gasoline.

Table 3: Safety-relevant characteristics hydrogen in comparison with methane and gasoline (Alcock 2001)

Fuel Properties	Hydrogen	Methane	Gasoline
Lower Flammability Limit (LFL) (vol% in air)	4	5.3	1
Upper Flammability Limit (UFL) (vol% in air)	75	15	7.8
Autoignition temperatures (°C)	585	540	228-471
Detonability limits (Lower limit LDL – vol% in air)	11-18	6.3	1.1
Detonability limits (Higher limit HDL – vol% in air)	59	13.5	3.3
Maximum burning velocity (m/s)	3.46	0.43	-

Hydrogen safety can be related to several phenomena, below few phenomena have been discussed that can expedite the loss of containment of hydrogen from the CGH2 storage tanks.

2.5.1 Dispersion

The properties of hydrogen previously mentioned make it safer than the hydrocarbons in some situations but could be more dangerous in others. Starting with leak characteristics, due to the lightest and smallest molecule of hydrogen the tendency to escape from the small leak in the tanks is much higher than other fuels. As a result, the leak in the high pressured tank in the case of CGH2 the hydrogen leak will be 2.5 times faster than methane (Alcock 2001). This indicates that any breach in the compressed hydrogen system would cause an uncontrollable dispersion in the environment around it and thus increasing the risk factor substantially.

2.5.2 Embrittlement

This phenomenon considers the hydrogen diffusion into the metals used to build the storage equipment such as metallic tanks (Wurster 2016). Thus, the metal integrity is affected and the material becomes more brittle which might lead to cracking. Three factors affect the formation of this phenomenon. First, the environment which reflects the exposure quantity, form, and conditions of hydrogen. Second the type of material used in the tank, and third, the field type such as mechanical, electrochemical, and operating conditions (Ustolin, Paltrinieri et al. 2020). The source of hydrogen to initiate this phenomenon can be from two types (Popov, Lee et al. 2018). Internal hydrogen embrittlement is the result of hydrogen inside the metal during the manufacturing process. Hydrogen environmental embrittlement where hydrogen enters the material from the hydrogen. This could be the potential risk involved when considering the loss of integrity of compressed hydrogen tanks. The hydrogen diffuses in the material in form of ions and when dealing with gaseous hydrogen it is not easily absorbed by the metal. Although, the temperature change can cause the gaseous hydrogen molecules to dissociate into atoms and generate the possibility to diffuse into the material and undergo embrittlement.

2.5.3 Storage system hazards

Hydrogen can be stored in both gaseous and liquid forms. To facilitate the storage network many sub-systems are integrated to develop a complete hydrogen storage system. When the system reached the multistage subcomponents level the possibility of hazards also increases related to the integrity and functioning of the equipment involved. The network may consist of pressurized tanks, compressors, pressurized pipelines, pressure valves, and hoses to fill or refill the tanks. All these types of equipment are subject to a certain level of risk when operating at high pressure for instance leak of the valve, material defect, or tank rupture and leak. All scenarios could lead to some serious consequences of high-pressure waves, leaks, fireball, or explosions.

2.6 Bow-tie

Given the possibility of the risk involved in the compressed hydrogen system and due to the erratic nature of the hydrogen, risk management for hydrogen technologies is required. There are several risk management methods available to analyze and assess risk and similarly, the bow-tie method is one of the most employed techniques in the industry. The bow-tie is the combination of the Fault Tree Analysis, Event Tree, Cause Consequence Diagrams, and Barrier thinking methods (de Ruijter and Guldenmund 2016) as shown in figure 2. In a typical bow tie, the left side represents the cause of the critical event which is usually analyzed by fault tree analysis where the 'top event' responsible for the accident is determined. On the right-hand side, the results of the critical event are analyzed by breaking them down into series of consequences using event tree analysis. In the thesis,

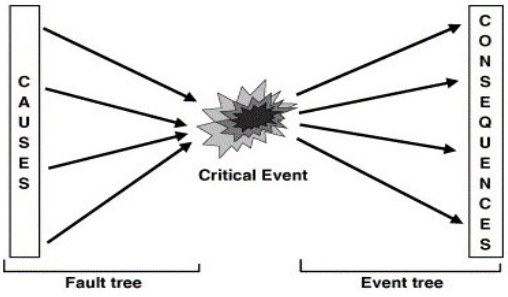

Figure 2: Bow-tie general scheme (De Dianous and Fievez 2006)

the analysis conduction will take place on the right-hand side of the bow-tie and modeling the consequence which will be discussed later in the coming chapters. The use of fault and event tree breakdowns the risk involved in multiple steps allowing the risk analysis to be conducted in detail (de Ruijter and Guldenmund 2016). Based on the bow-tie model, a method to identify the major accident hazards in process industries is devised known as Identification of major accident hazards (MIMAH) (Delvosalle, Fievez et al. 2006).

2.6.1 Causes

In general, the nature of the causes could be different from system to system. The left side and the first step of the bow-tie identifies the cause that leads to the critical event. This is the first step of the analysis; the significance of the step is important as it breaks down the fault into subsets responsible for the failure.

For compressed hydrogen storage system, the cause of failure can be the failure of the pressurized equipment, breach in the pressurized pipeline, loose hose connection while refiling of tanks, pressure valve leak or malfunction, failed venting system, fracture in a tank, and collision of transportation trucks (Ustolin, Paltrinieri et al. 2020). Similarly, in the case of liquid hydrogen, the hydrogen is liquified at low temperature, humid air around the equipment can solidify on the components of the system such as relief valves (Ustolin, Paltrinieri et al. 2020), boil-off excessive pressure can cause rupture or explosion, liquid hydrogen spill during filing might undergo ignition after forming a combustive mixture with air under certain conditions (Royle and Willoughby 2009) and collision of transportation trucks.

2.6.2 List of events

The causes of the failure give rise to an event or series of events that could be critical. The central part of the bow tie focuses on critical events, the type of events that signifies the loss of physical integrity (LPI) and loss of containment LOC (Delvosalle, Fievez et al. 2006). In (Delvosalle, Fievez et al. 2006) MIMAH technique was used in the Accidental Risk Assessment Methodology for Industries (ARAMIS) project on the ethylene oxide cylinder vessel to identify the ‘major accidents’. In the analysis, the worst analysis was taken as the likelihood of the occurrence of the worst accidents on the equipment under analysis with no safety system fitted. As a result of this approach, the critical event identified can be considered for the CGH2 storage system.

The analysis was presented in series of step used in the MIMAH and identified several critical events, but the ones that relate to the CGH2 system are the catastrophic rupture of the tank, leak from the gas pipe, breach in the shell, and start of fire (Ustolin, Paltrinieri et al. 2020). A total of three breach sizes has been considered in the analysis on both tank shell and pipe as shown in table 4, the values are of great use for the leak consequence modeling.

Table 4: Breach and leak size tank and pipe of the storage system (Delvosalle, Fievez et al. 2006)

Size of leak	Diameter of the breach in the shell	Diameter of the leak in the pipe
Small	10 mm	10% of the pipe diameter
Medium	35–50 mm	22-44% of the pipe diameter
Large	100mm	Full bore rupture

2.6.3 Consequences

The right part of the bow-tie is based on event tree analysis which identifies the possible consequences involved in the critical event. As discussed earlier, the ignition energy of hydrogen is relatively lower than other traditional fuels and this energy can be easily fulfilled by the mechanical sparks, sparks from the truck engine, or electrostatic discharges (Ordin 1997).

2.7 European Agreement Concerning the International Carriage of Dangerous Goods by Road (ADR)

The dangerous goods are not safe to transport under the normal condition concerning the goods handling, equipment design, and construction, transport routes. They are classified as either prohibited to transport by roads or permitted to transport on road under a certain set of conditions and regulations. To transport a certain type of fuel like CGH2, a company must adhere to compliance with the ADR regulations.

When it comes to CGH2, with regards to with which pressure and quantities there are no specific limitations and guidelines by the Norwegian government when transporting it by road. With respect to ADR, hydrogen is categorized in the list of dangerous goods as "Extremely Flammable Gas" H220 or as compressed gas, H280. It falls in ADR class 2, classification code 1F, UN# 1049, Class 2.1. Class 2 is further classified into flammable, non-flammable & non-toxic, and toxic. The .1 represents the compressed hydrogen belongs to the flammable gases category. The labels shown in figure 3 are the ones used on the truck transporting CGH2.

Figure 3: ADR labels for CGH2

The UN-Model regulation, ADR, and the European Transportable Pressure Equipment directive (1999/36/EC– "TPED") limit the transport of CGH2, restricts the increase in payload of hydrogen trailers, and the cylinder/tube volumes by 450 l/3,000 l.

In Norway, the details regarding the tunnel routes, driver competence, and drivers' cabin safety have been clearly mentioned and are being followed. In tunnels, restrictions apply to categories tunnels with categories B, C, D, and E when transported using a pressurized tank. In Norway, the restrictions of transportation through tunnels apply to subsea tunnels between Ellingsøy and Valderøy near Aalesund during the time duration of 0600 to 2400. To transport hydrogen at Hvalertunnelen requires Road traffic central's permission. In the case of driver competence, the Norwegian public Roads Authority is responsible for the regulations of ADR driver and vehicle certification. As per the ADR, the driver must hold an ADR certificate (section 8.2.1, ADR/RID 2017). ADR Book Chapter 5 can be used to develop consignment procedures. In section 5.4.1, ADR instructions about handling of emergencies and accidents in case of an accident during transportation. Lastly, for driver cabin safety in chapter 9 'requirements* concerning the construction and approval of vehicles' it is mentioned under sections 9.3.3 and 9.3.4 the drivers' cabin shall be separated by a continuous wall from the carriage section. The important details assigned by ADR for CGH2 are mentioned in table 5, the table gives a holistic view of the nature of the material being dealt with.

Table 5: CGH2 ADR specifications (ADR 2017)

Description	Details	Comments
UN number	1049	
Name	Compressed Hydrogen	
Class	2	Gases
Classification	1F	1 – compressed gas having a critical temperature less than -50 ^{O}C F – Flammable
Labels	2.1	As shown in figure 3
Special Provisions	660 662	Guidelines for fuel gas containment systems Guidelines for tank protection, labeling, and packing details
Packing instructions	P200	Specifications of pressure receptacles
Portable tank and bulk container instructions	M	M - substance may be carried in UN MEGCs (UN multiple-element gas container)
Tank codes for ADR tank	CxBN(M)	
Vehicle for tank carriage	FL	i - A vehicle intended for the carriage of flammable gases in fixed tanks or demountable tanks with a capacity exceeding 1 m^3 or in tank-containers, portable tanks, or MEGCs with an individual capacity exceeding 3 m^3; or ii - A battery vehicle with a total capacity exceeding 1 m^3 intended for the carriage of flammable gases;
Tunnel code	B/D	Tank carriage: Passage forbidden through tunnels of category B, C, D, and E; Other carriages: Passage forbidden through tunnels of category D and E
Special provisions for carriage: Loading and unloading	CV9, CV10, CV36	Detail regarding the horizontal and vertical placement of tanks on a truck with respect to dimensions
Hazard identification No.	23	Flammable gas

3 Research Design and Methods

In this chapter, the approach adopted to analyze the risk analysis concepts and experimental data to streamline the simulation data and developing a model is discussed. First, the review details highlight the methods used to filter the articles searched using a specific set of keywords and search engines. Next, the employed risk assessment concepts that aid the safety analysis and the selection of the software for the computational fluid dynamics (CFD) modeling activity are discussed. Lastly, the specifications of the modeled equipment are described together with the numerical simulation settings.

3.1 Methodology Steps

Hydrogen safety depends on how competently it is handled during the design, manufacturing, and operations phases. At the design phase, the detailed analysis of the documentation and literature with the combination of simulations supports the initial engineering design phase. Contributing to selection and integration of safety equipment in the design, selection of material for construction, quality standards, certification and standards specifications, design in line with ADR regulations, and preemptive resource planning. Then next comes the execution phase for the manufacturing of the trucks and later operations.

As the thesis work stands and contributes to the first phase the design phase of the project. The consequence analysis results provide important indications in terms of pressure produced due to the blast wave that must be considered during the designing of the safety barrier to be placed behind the driver cabin as well as the blast wave propagation behavior in terms of pressure, temperature, and velocity with respect to distance travelled. The additional barrier is part of ADR regulation and escalates the safety of the cabin in case of tank rupture and explosion. However, the results also give an insight into the phase of truck operations regarding tank rupture overpressure effect on the surroundings and understanding of what the company is dealing with during transportation.

The following steps briefly define the methodology strategy implemented in the thesis work:

- Identification of risk assessment concepts to support the consequence analysis.
- Selection of experimental data of the tank rupture scenario from the literature (mentioned in table 6)
- Modeling the experiments by means of a CFD code.
- Grid independence analysis is carried out.
- The results are compared with the experimental results and CFD analysis outcomes retrieved from the literature to validate the model developed in this thesis.
- Using the validated model configuration to model large-scale tank rupture.
- Separation distances at which temperature and pressure effects have the potential to cause injury (minor and severe) or fatality are estimated from the CFD analysis results.

3.2 Literature review

A narrative review was adopted to analyze and summarize the most relevant studies in the literature. This type of review can be very useful in gathering together a volume of

literature in a specific subject area and synthesizing it (Sylvester, Tate et al. 2013). This approach maps and provides the foundation data for the study.

In this thesis following keywords were used on the databases of ORIA (2021) and Google Scholar (2021):

- Compressed Hydrogen
- Hydrogen Safety
- Blast wave and fireball
- Hydrogen storage
- Risk assessment
- Consequence analysis
- CFD model

3.3 Risk Analysis Concepts

Hydrogen handling is primarily limited to trained personnel and companies. To use hydrogen in transportation means the interaction will be in varying environments, with personnel nearby and different conditions so it must be handled with no risks and a high degree of confidence.

3.3.1 Risk

Risk is the product of probability and consequences (Kaplan and Garrick 1981). A person may be harmed if exposed to a hazard i.e., hydrogen tank rupture due to a vehicle accident. This risk here can be taken as a risk in terms of the fatality rate. Nonzero probability of failure exists in case of CGH2 tank rupture in a fire and rupture in the open atmosphere leads to the destructive blast wave and fireball formation with the possibility of developing diameter reaching tens of meters (Kashkarov, Li et al. 2020). The blast wave formation has the tendency to cause fatalities and injuries of human life and building around it. Due to tank rupture, the risk of fatality per vehicle per year can be evaluated as (Dadashzadeh, Kashkarov et al. 2018):

$$Risk_{fatality} = Rupture\ frequency\ x\ N, \quad (1)$$

The equation above is supported by the probabilities of events taking place on hydrogen-powered vehicles using type IV tanks and the concept can be considered for the analysis under study. The rupture frequency can be determined using published data of events taking place in the rupture process. Whereas N represents the number of fatalities and is assessed as (Dadashzadeh, Kashkarov et al. 2018):

$$N = N_0\ x\ A_{effect} \quad (2)$$

N_0 represents the population density of the accident location and A_{effect} area within the blast wave.

The risk for this specific consequence of blast wave can be calculated using the above equations and the data available.

The calculated risk can be interpreted to determine the harm criteria of the generated blast wave pressures on the basis of three harm thresholds defined in (Kashkarov, Li et al. 2020). The three hazard regions are based on overpressures, i.e., no harm, injury, and fatality. The 'no harm' zones represent the region where the blast overpressures are below 1.35 kPa, the 'injury' zone represents the blast overpressures ranging from 1.35 to 16.5 kPa, and the 'fatality' zone having is classified into two further regions based on the range of blast wave overpressure. The zones having overpressures from 100 kPa and higher are 'fatality zone' and the zones having overpressures ranging from 16.5 to 100 kPa are

'Serious injury'. Figure 4 shows the hazard zones classifications on the blast wave propagated after the CGH2 tank rupture.

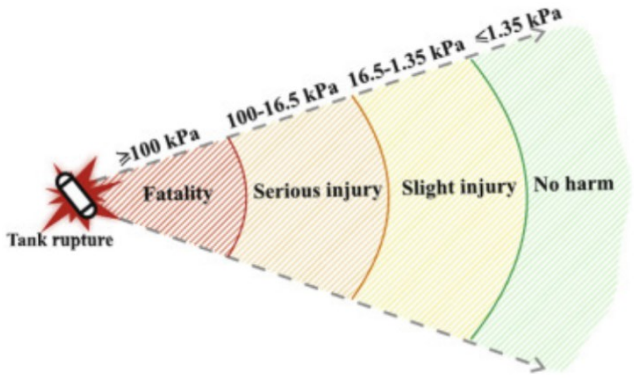

Figure 4: Hazard region classification on blast wave generated due to tank rupture (Kashkarov, Li et al. 2020)

In the fatality zones, people would be prone to more fatal injuries and lung hemorrhage, while the serious injury zones include eardrum rupture and internal injuries. Based on the hazard zone classified by (Kashkarov, Li et al. 2020), the results achieved from the CFD study portrait the distances covered by the blast wave having pressures above 100 kPa for risk estimation and below 1.35 kPa to determine safe distance. In future, the expected harmful effects to human life in the case of tank rupture are shown in the results part against the blast wave pressures achieved with respect to distances travelled.

3.4 Consequence analysis

Consequence analysis examines the potential effects of hazards to the environment, equipment, asset, and human life. The sequences of events of incidents are identified to determine the hazard consequence. To present the hydrogen safety aspects the bow tie method is utilized to identify the possible hazards, faults, critical events, and consequences involved. The main objective for the modeling of consequence falls within the right hand side of the bow-tie i.e., tank rupture. In the thesis, the critical event, i.e. the tank rupture is modeled and analyzed.

In the case of the CGH2 tank under analysis, consequences of the catastrophic tank rupture are usually the blast wave and fireball. In figure 5 the sequence of tank rupture was presented by (Dadashzadeh, Kashkarov et al. 2018) who depicts the initiation of this accident from the starting events and leading to the consequences. The left side shows the list of three causal events and one of these could be the initiating event for the tank rupture. The first consequence (blast wave and dispersion) is under analysis in this study.

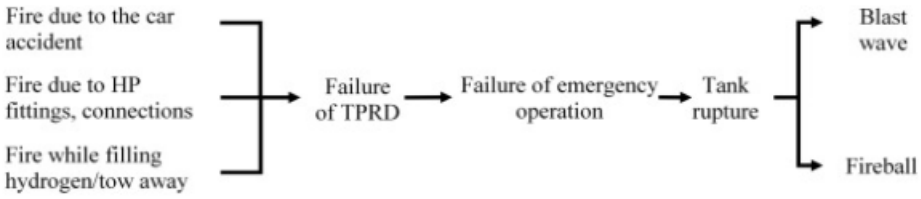

Figure 5: Tank rupture events (Dadashzadeh, Kashkarov et al. 2018)

3.5 CFD analysis

3.5.1 Ansys Fluent

The software used to model the consequences of the tank rupture is Ansys Fluent. Ansys Fluent is a CFD code. The blast wave and dispersion of hydrogen are determined in an open environment in case of tank rupture. The range of the blast wave and dispersion in terms of pressure and temperature is to be determined. Ansys Fluent uses suitable governing equations to estimate the loss of containment consequences.

The governing equations in the model facilitating the simulation involve Favre averaged compressible conservation equations of mass and momentum shown in equation 3 and 4 below (Kim, Shentsov et al. 2017):

$$\frac{\partial \rho}{\partial t} + \frac{\partial}{\partial x_j}(\rho u_i) = 0 \tag{3}$$

$$\frac{\partial \bar{\rho} u_i}{\partial t} + \frac{\partial}{\partial x_j}\left(\bar{\rho} u_i u_j\right) = -\frac{\partial \bar{\rho}}{\partial x_i} + \frac{\partial}{\partial x_j}(\mu + \mu_t)\left(\frac{\partial u_i}{\partial x_j} + \frac{\partial u_j}{\partial x_i} - \frac{2}{3}\frac{\partial u_k}{\partial x_k}\delta_{ij}\right) + \rho g_i \tag{4}$$

The student version R1 2021 is being used for all the simulations. This version has a free license and is downloadable from the official Ansys website. The student version has few limitations, the most important is related to the sizing of the grid. The limit is the development of elements and nodes which is 512,000 cells/nodes. This limit may have some effect on the accuracy of the CFD since finer meshes produce more accurate results. Second, the number of bodies that can be imported into the geometry is limited to 50. This limitation has no effect on the model developed in the thesis as it consists of only two bodies.

To simulate the flow characteristics of the two-equation model, the k-epsilon (k-ε) turbulence model has been implemented (Kim, Shentsov et al. 2017). The realizable model predicts accurately the spreading rates of both planer and round jet.

3.6 Case study description

In this section, the scenario analyzed in the model is described. Two cases have been investigated a small-scale CGH2 tank (Type IV) and a large-scale CGH2 tank (Type IV). Both CGH2 tanks rupture are modeled in the thesis and the generated blast wave is analyzed.

The selection of the above-mentioned scenario is due to the fact that under thermal loads CGH2 Type IV tanks tend to degrade and pressurize (Dadashzadeh, Kashkarov et al. 2018). Additionally, these types of tanks as discussed above in the objective and section 2.3.1 are favored for truck storage because of their high-pressure bearing capabilities and lightweight. The time to rupture from the start of a fire nearby is around 6 to 12 min, without the application of tank thermal protection and pressure safety valve (Weyandt 2005).

Similar conditions are set when setting the initial model. The depressurization of the CGH2 tank content at the ruptured pressure and temperature before its rupture is simulated. The tank is placed 0.2 m above the ground in an open environment. A small-scale tank tested during the experiments of (Zalosh and Weyandt 2005) was simulated to validate the model and then using the validated model configuration to modeled the large-size tank rupture.

3.6.1 Specifications (tank data)

3.6.1.1 Small-scale tank

The tank specifications are adapted from (Zalosh and Weyandt 2005) where a fire exposure test was conducted on a Type IV tank with no pressure safety valve installed. The experimental test conducted by (Zalosh and Weyandt 2005) was to identify the behavior of the blast wave and fireball produced upon tank rupture. In the thesis, only the blast wave is analyzed. The tank specifications are collected in table 6.

Table 6: CGH2 tank specifications (Zalosh and Weyandt 2005)

Material (composite)	Type HGV-4
Volume	72.4 L/ 4420 in^3
Type	HGC-4 Type IV
Initial Pressure	34.6 MPa
Initial Temp	27 ^{O}C
Mass H2	1.64 kg
Length	0.84 m/33 in
Diameter	0.41 m/16 in
Ruptured Pressure	35.7 MPa
Ruptured Temp	39 ^{O}C

Figure 6: Experimental Type IV tank (Zalosh and Weyandt 2005)

3.6.1.2 Large-scale CGH2 tank

The tank model specification has been taken from a Norwegian manufacturing company (UMOE 2018) shown in table 7. The tank data provided by the manufacturer mentioned above, have the EN 12245-3, ADR / TPED approval.

Table 7: Large-scale CGH2 tank specifications (UMOE 2018)

Tank type	Standard type IV pressure vessels
Working Pressure (bar)	200
Tank Length (m)	5.860
Tank Diameter (m)	0.708
Hydrogen Capacity (kg)	25

The purpose to develop this large-scale model is to evaluate the effect of the blast wave on a large-scale tank if used in real-life operations.

3.6.2 Geometry, Mesh, and System Boundaries

A two-dimensional (2D CFD study is conducted in the thesis. Two different tank geometries were drawn by following the specifications of the above-mentioned tank (tables 6 & 7). The domain in which the tank is placed is an open environment, and the rectangular shape has been adopted to facilitate the meshing process. The dimensions of the domains are 35 X 20 m for the small-scale tank adopted from literature and 70 x 40 m for the large-scale tank. the domain dimensions were chosen according to experimental data since the blast

wave propagated within a shorter distance. The bottom edge of the domain simulates the ground, thus is considered solid. The tank is placed horizontally at the center of the domain. In this phase of integration of two bodies, it is important to define in the model that the domain body has hollow space where the tank is to be placed as in this geometry one body (tank) is within the other body (domain). This function is done by using the Boolean function which subtracts the domain body from the tank body and changing the type of domain to 'add frozen'. Such arrangement allows in solver to define different types of fluids in different bodies, like hydrogen and air inside tank and domain, respectively. Figure 7 shows the geometry drew in the DesignModeler and the detailed geometry picture including DesignModeler settings attached in appendix 1.

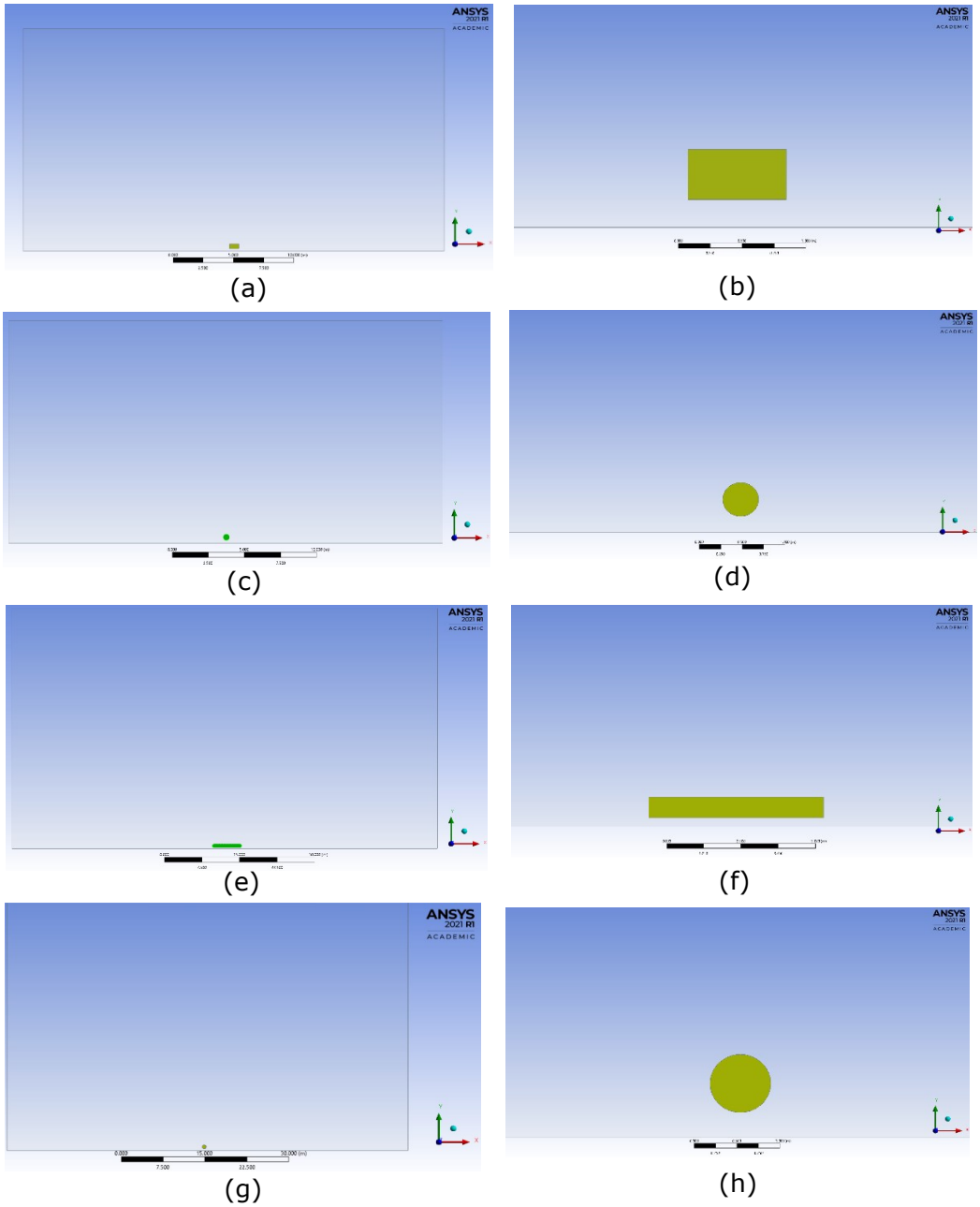

Figure 7: (a) Geometry of longitudinal axis of small-scale CGH2 tank (b) Enlarged portion of the longitudinal axis of small-scale tank (c) Geometry of transversal axis of small-scale CGH2 tank (d) Enlarged portion of the transversal axis of small-scale tank (e) Geometry of longitudinal axis of large-scale CGH2 tank (f) Enlarged portion of the longitudinal axis of large-scale tank (g) Geometry of transversal axis of large-scale CGH2 tank (h) Enlarged portion of the transversal axis of large-scale tank.

The next step is to develop the mesh and name boundaries in the mesh option of fluent. Keeping in mind the limitation of the number of cell numbers in Ansys student, the mesh element size has been selected carefully. The mesh on the tank is finer relative to the domain as the tank area is much finer than the domain mesh. Because the area of the tank is extremely small compared to the entire domain, the mesh must be finer in the tank region to increase the convergence and accuracy. The mesh developed on the domain and tank can be seen in figure 8 and the detailed mesh pictures are attached in appendix 1:

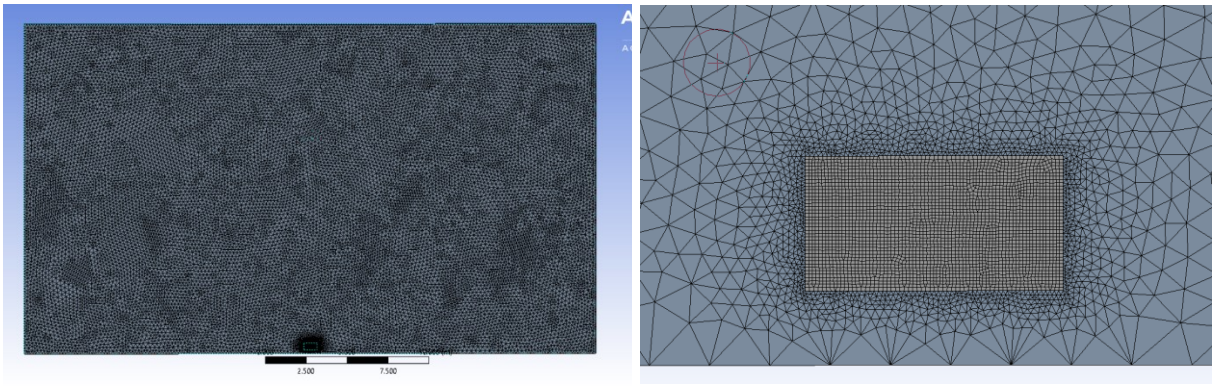

(a) (b)

Figure 8: (a) mesh of the entire domain and (b) enlarged portion of the tank.

For the small-scale CGH2 tank the mesh minimum element size is 0.2 m, the growth rate 1.2, and the number of elements is 42,503. The large-scale tank (second case study) mesh minimum size is 0.24 m, the growth rate 1.2, and the number of elements is 113,886.

3.6.3 Solver details

The model is pressure-based and transient with the gravity effect on Y-axis set as -9.81 m/s^2. In the models, the energy equations option is activated and the k-ε turbulence model with standard wall functions is selected. Hydrogen is added as new material from the Fluent library in this model, while air is implemented as default. In fact, the domain material is air, and it is changed in the tank zone to hydrogen. The solution methods and transient formulation would be simple and first-order implicit. Similarly, solution controls were kept standard. The operating conditions (temperature and pressure) in the domain are defined when initializing the simulation by setting the values listed in tables 6 & 7 for both models. The time step size of 1.0e-06 s and the total simulation time of 0.1 s were selected.

3.6.4 Assumptions

Several assumptions have been considered while developing the model in terms of geometry design, fluids operating conditions. Following are the assumptions:

- The tank rupture scenario was simulated as complete and instantaneous destruction of the CGH2 tank wall.
- The domain initial conditions are set as ambient conditions for pressure and temperature of 101325 Pa and 288 K, respectively.
- No effects of wind in the domain.
- Hydrogen in the CGH2 tank is considered an ideal gas (Molkov, Cirrone et al. 2021).
- Hydrogen combustion is neglected.

4 Results

This chapter presents results for the consequence analysis of blast wave upon tank rupture. The wave propagation along both the tank longitudinal and transversal axes are presented. The profiles of pressures, temperatures, and velocity are reported.

4.1 Selection of Literature

The selection of literature was solely directed towards the consequence modeling of the compressed hydrogen tank. The narrative review summarizes the previously published data on the CGH2 tank and the consequences related to its catastrophic rupture. The review resulted in specifying the existing studies on the parameters involved in the consequences analysis and modeling of CGH2 tanks. Table 8 lists the most important articles used in the thesis and a brief discussion of the selection criterion.

Table 8: Important articles and selection criteria

Selected Article	Selection Criteria
(Delvosalle, Fievez et al. 2006)	Major accidents in compressed cylinder identified and tank breach diameters details
(Zalosh and Weyandt 2005)	Type-IV compressed hydrogen fire exposure experimental test, tank design, and blast wave details
(Kim, Shentsov et al. 2017)	Details for Ansys Fluent model with respect to tank geometry and simulations
(Molkov, Cirrone et al. 2021)	CFD model details for blast wave dynamics after compressed hydrogen gas rupture in an open environment

4.2 Analysis of Blast wave due to tank rupture

The model specification, geometry, and numerical settings were mentioned in section 3.6. Here, the pressure, temperature, and velocity profiles are presented. These profiles are important to understand the behavior of the blast wave effect on the tank surrounding and contribute to the main objectives of the thesis. The grid independence study is presented initially for the model which is followed up by the results profiles. First, the results achieved for the small-scale CGH2 tank model replicated from the literature in sections 4.2.1 and 4.2.2 will be presented showing blast wave along the longitudinal and transversal axes, respectively. Then, in sections 4.2.3 and 4.2.4, the results show the large-scale tank rupture blast wave propagation along the longitudinal and transversal axes.

4.2.1 Small-scale CGH2 Tank (longitudinal axis)

4.2.1.1 Grid Independence Study

Obtaining confidence in the model grid dependency is important. With the grid independence test, it is found to what extent the mesh must be refined to achieve a reasonable level of tolerance. The test is done by reducing the minimum cell size and comparing the results obtained with the different grids. Table 9 shows the comparison of

the three types of mesh used for the model and the results achieved on the respective mesh.

Table 9: Grid independence test comparison

Mesh Type	Elements	Pressure (kPa) at 1.5 e-3 s and 0.86 m from the tank	Temp (K) at 1.5 e-3 s and 0.86 m from the tank	Error (%) (pressure)	Error (%) (temperature)
Coarser	8501	238.03	102.44	-	-
Medium	28173	134.73	76.88	55.42	28.50
Fine	42503	137.00	77.30	1.67	0.54

Figure 9 shows the graphical demonstration of the grid independence test for the model.

The refinement ratio must be higher than 1.3, according to the Richardson extrapolation (Roache 1993).

Refinement ratio of fine and medium mesh $= \frac{\text{Fine mesh elements}}{\text{Medium mesh elements}} = 1.51$

Refinement ratio of medium and coarse mesh $= \frac{\text{Medium mesh elements}}{\text{Coarse mesh elements}} = 3.31$

The refinement ratio is acceptable to conduct analysis and the relative error reduces further as the mesh turns into a finer mesh.

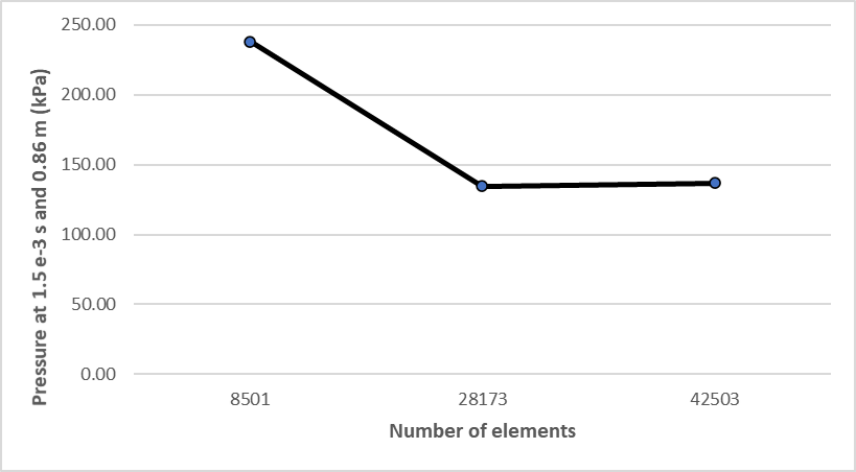

Figure 9: Grid independence test plot

4.2.1.2 Pressure profile

Figure 10 shows the behavior of the pressure wave generation and propagation with respect to time upon the CGH2 tank rupture at pressure 35.7 MPa as mentioned in table 6. At 7.0e-4 s, the wave propagates out to the surrounding, hits the ground, and reflects as expected. At 9.7e-4 s, the wave at the ground applies overpressure of 25.86 MPa, the reflection creates another wave that goes upwards towards the head of the blast wave. Consequently, at 3.3e-3 s the wave shape adopts the hemispherical shape and continues to expand. The ground reflection of the second wave is more visible.

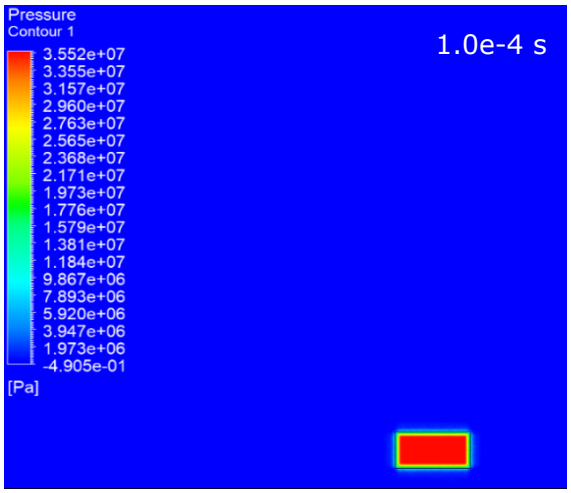
Pressure
Contour 1
3.552e+07
3.355e+07
3.157e+07
2.960e+07
2.763e+07
2.565e+07
2.368e+07
2.171e+07
1.973e+07
1.776e+07
1.579e+07
1.381e+07
1.184e+07
9.867e+06
7.893e+06
5.920e+06
3.947e+06
1.973e+06
-4.905e-01
[Pa]
1.0e-4 s

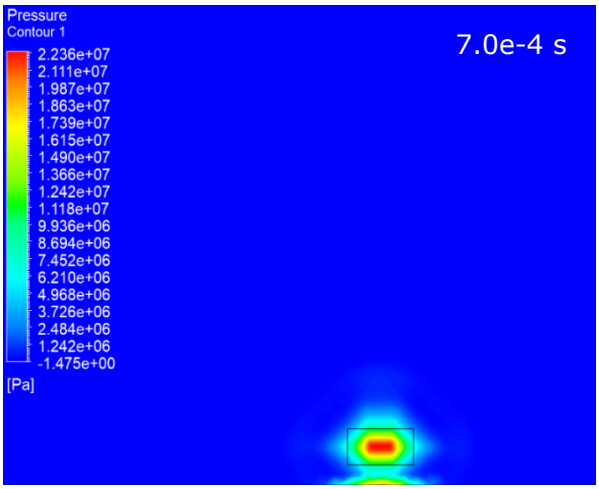
Pressure
Contour 1
2.236e+07
2.111e+07
1.987e+07
1.863e+07
1.739e+07
1.615e+07
1.490e+07
1.366e+07
1.242e+07
1.118e+07
9.936e+06
8.694e+06
7.452e+06
6.210e+06
4.968e+06
3.726e+06
2.484e+06
1.242e+06
-1.475e+00
[Pa]
7.0e-4 s

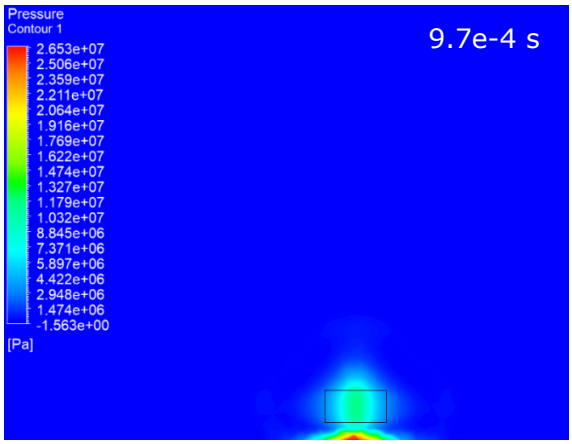
Pressure
Contour 1
2.653e+07
2.506e+07
2.359e+07
2.211e+07
2.064e+07
1.916e+07
1.769e+07
1.622e+07
1.474e+07
1.327e+07
1.179e+07
1.032e+07
8.845e+06
7.371e+06
5.897e+06
4.422e+06
2.948e+06
1.474e+06
-1.563e+00
[Pa]
9.7e-4 s

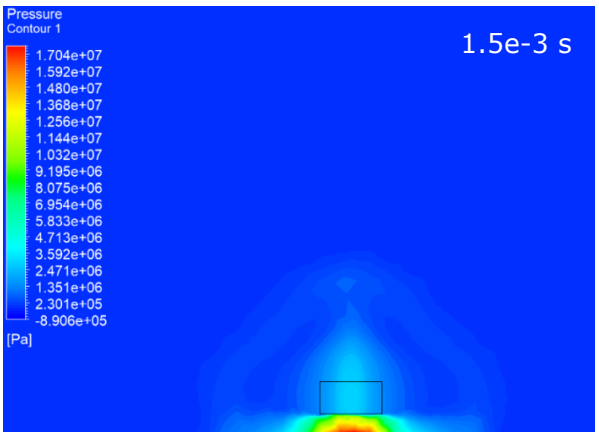
Pressure
Contour 1
1.704e+07
1.592e+07
1.480e+07
1.368e+07
1.256e+07
1.144e+07
1.032e+07
9.195e+06
8.075e+06
6.954e+06
5.833e+06
4.713e+06
3.592e+06
2.471e+06
1.351e+06
2.301e+05
-8.906e+05
[Pa]
1.5e-3 s

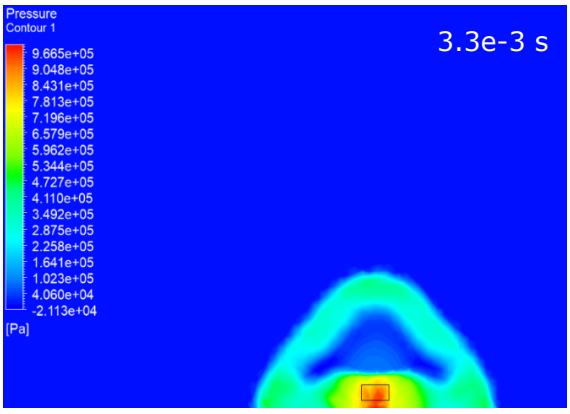
Pressure
Contour 1
9.665e+05
9.048e+05
8.431e+05
7.813e+05
7.196e+05
6.579e+05
5.962e+05
5.344e+05
4.727e+05
4.110e+05
3.492e+05
2.875e+05
2.258e+05
1.641e+05
1.023e+05
4.060e+04
-2.113e+04
[Pa]
3.3e-3 s

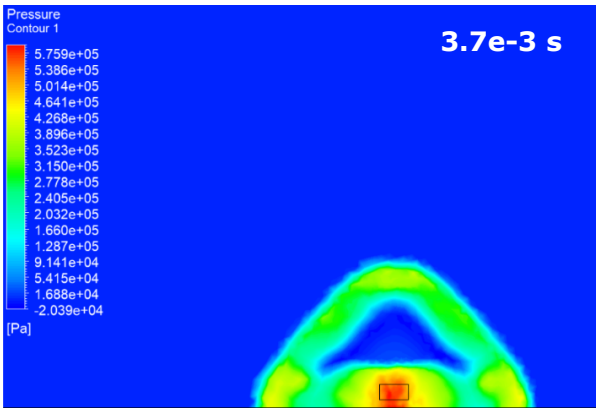
Pressure
Contour 1
5.759e+05
5.386e+05
5.014e+05
4.641e+05
4.268e+05
3.896e+05
3.523e+05
3.150e+05
2.778e+05
2.405e+05
2.032e+05
1.660e+05
1.287e+05
9.141e+04
5.415e+04
1.688e+04
-2.039e+04
[Pa]
3.7e-3 s

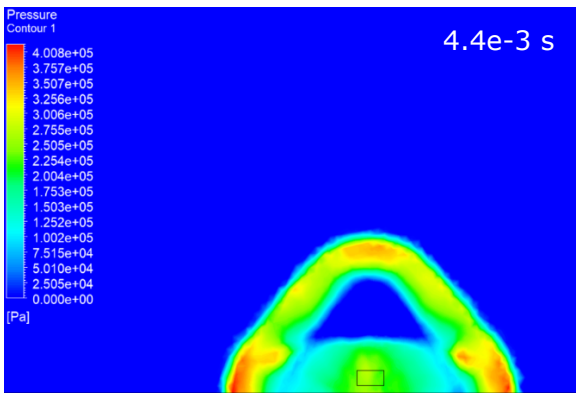
Pressure
Contour 1
4.008e+05
3.757e+05
3.507e+05
3.256e+05
3.006e+05
2.755e+05
2.505e+05
2.254e+05
2.004e+05
1.753e+05
1.503e+05
1.252e+05
1.002e+05
7.515e+04
5.010e+04
2.505e+04
0.000e+00
[Pa]
4.4e-3 s

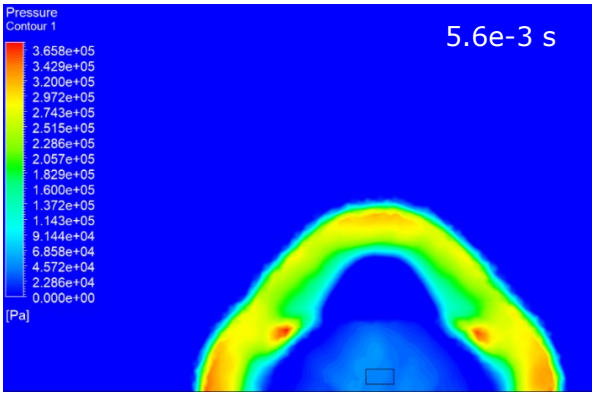
Pressure
Contour 1
3.658e+05
3.429e+05
3.200e+05
2.972e+05
2.743e+05
2.515e+05
2.286e+05
2.057e+05
1.829e+05
1.600e+05
1.372e+05
1.143e+05
9.144e+04
6.858e+04
4.572e+04
2.286e+04
0.000e+00
[Pa]
5.6e-3 s

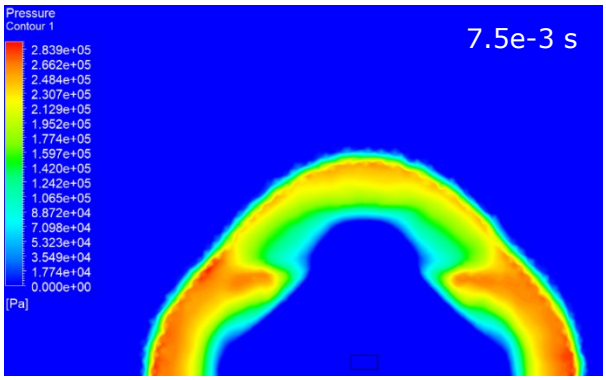

Figure 10: Pressure wave evolution at different time steps upon CGH2 rupture – Small-scale tank longitudinal axis

Later, at 4.4e-3 s the overpressure produced at the ground under the tank is reduced and the effect of the second wave ground reflection can be seen also on the sides of the waves perpendicular to the axis of the tank. At 7.5e-3 s the pressure reduces and the wave along with the second waves continues to disperse.

4.2.1.3 Temperature profile

Figure 11 shows the temperature profile of the blast wave following the same time intervals as shown in figure 10. At the initiation of the rupture the temperature in the surroundings begins to increase, the sudden temperature increase can be seen at 7.0e-4 s. This is due to the fact that the wave propagates and the air temperature increase due to adiabatic compression (Kim, Shentsov et al. 2017). The reduction in the temperature below ambient occurs due to the hydrogen expansion. The highest temperature of 622 K is observed at 1.5e-3 s, due to the propagation of the second wave formation at the ground. With the time progression, the outer hemispherical wave consists of high-temperature profiles as compared to the inside low-temperature region.

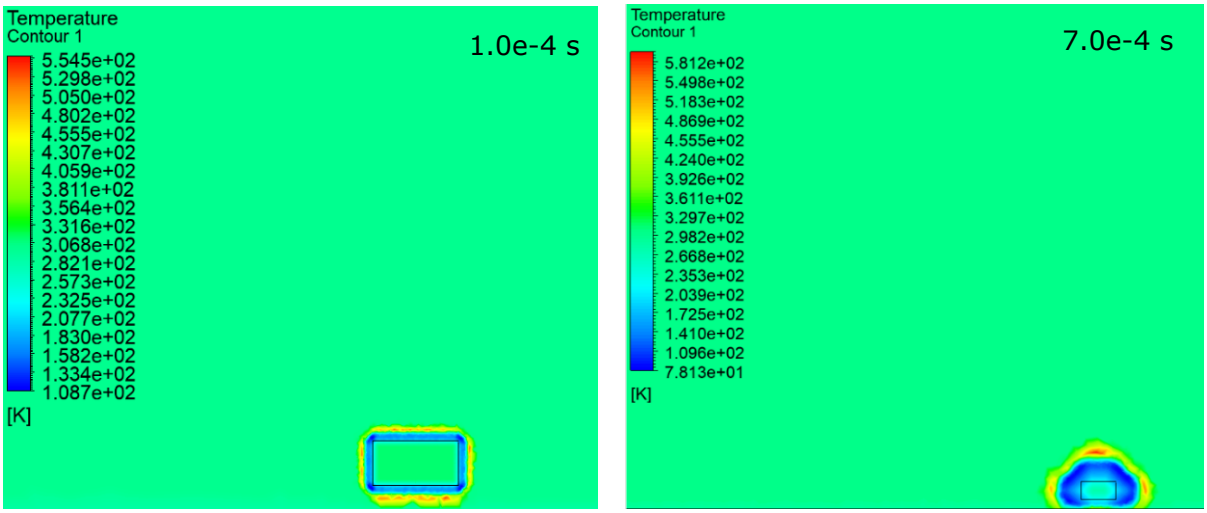

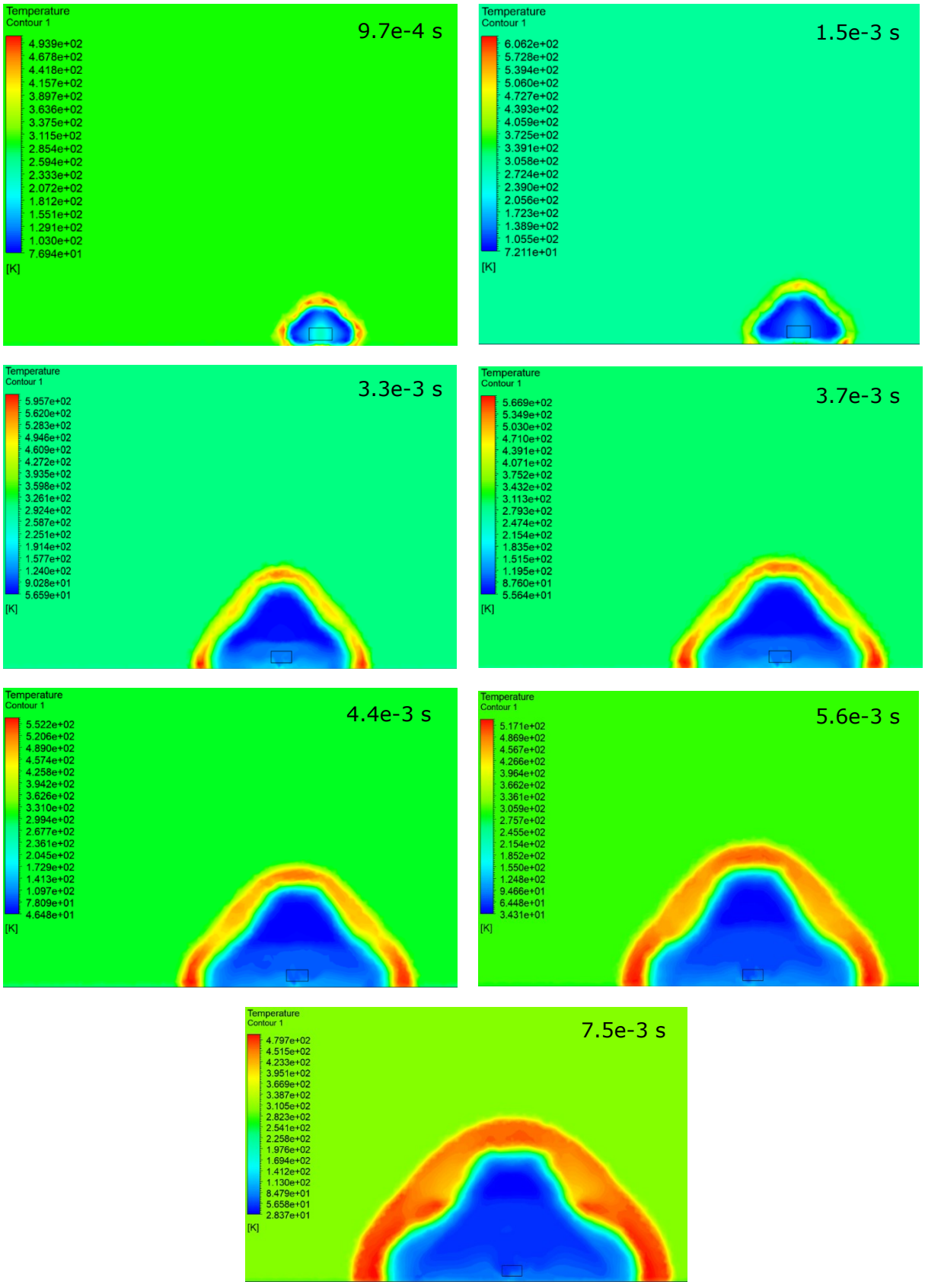

Figure 11: Temperature profile of to the domain at different time steps upon CGH2 rupture – Small-scale tank longitudinal axis

4.2.1.4 Velocity profile

Figure 12 shows the velocity profile of the blast wave following the same time intervals as shown in Figures 10 and 11. At 1.0e-4 s, velocity is the highest at 826 m/s, hydrogen releases from the high pressurized region of the tank. With time the wave propagates, and the velocity of the blast can be seen decreasing with time. However, at 5.6e-3 s the velocity of the second wave is visible and showing its impact on the sides of the initial wave.

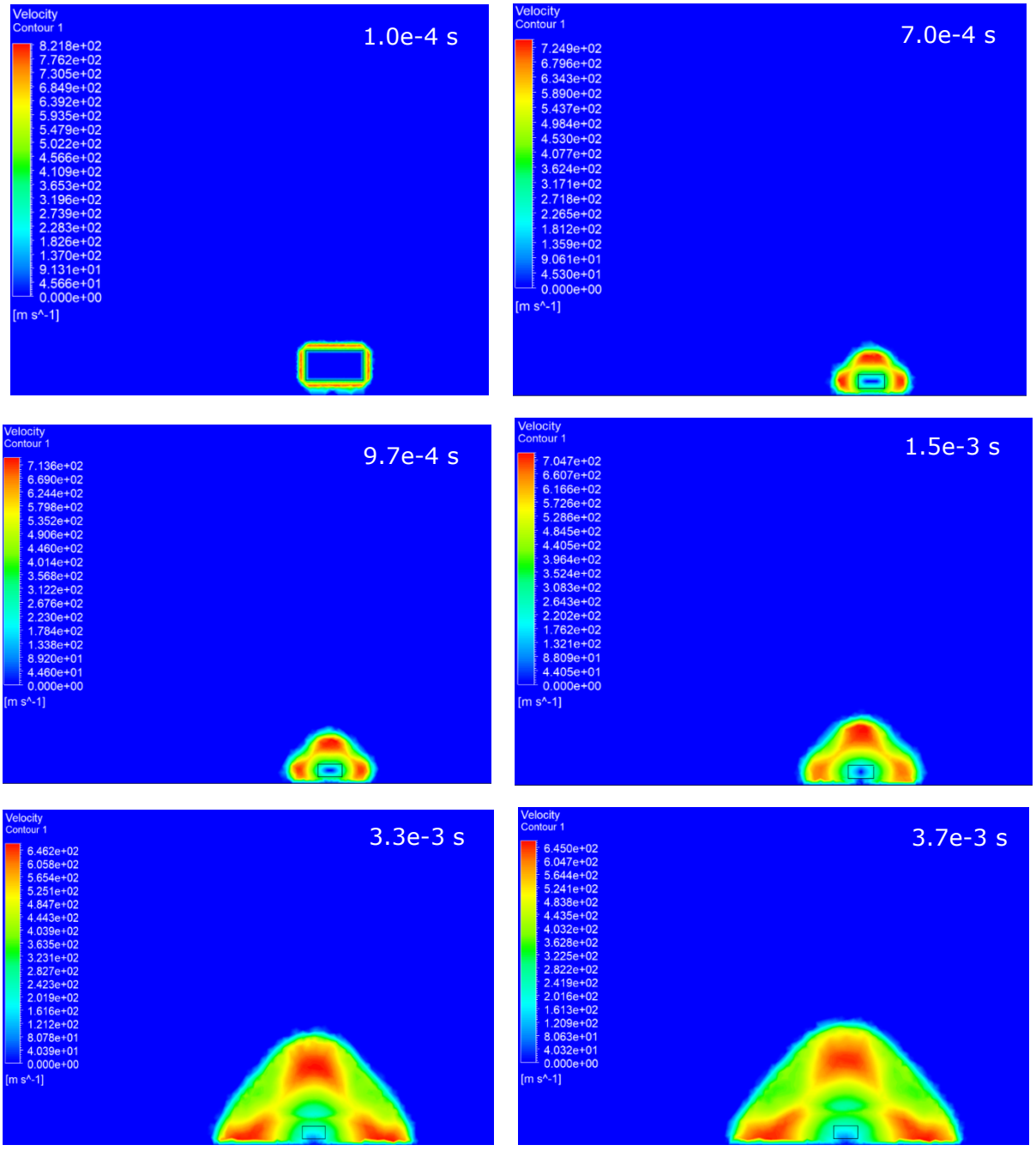

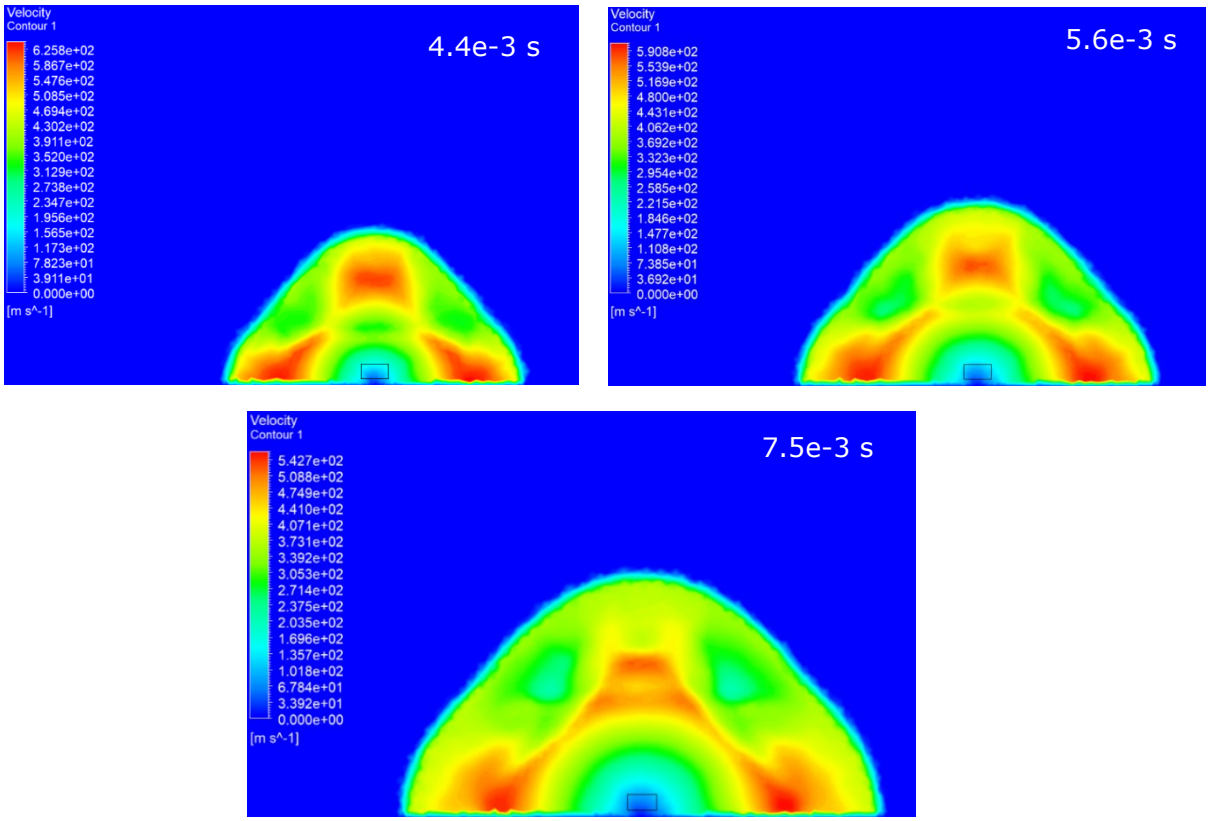

Figure 12: Velocity profile of the domain at different time steps – Small-scale tank longitudinal axis

4.2.1.5 Results comparison

The experimental test (Zalosh and Weyandt 2005) and simulation results (Kim, Shentsov et al. 2017) show the pressure values at certain distant points from the tank location. The thesis results are compared with the results achieved in the mentioned papers and are discussed in the discussion.

In the experimental test (Zalosh and Weyandt 2005) the tank was placed above the burner and after the fire exposure for 387 s, the tank ruptured at 35.7 MPa. To measure the pressure of the blast wave, three piezoelectric blast wave pressure probes at the elevation to the cylinder axis placed at distances of 1.9 m, 4.2 m, 6.5 m. Similarly, the blast wave results were simulated in (Kim, Shentsov et al. 2017) and compared pressure at the distances mentioned. The thesis results are compared with the results achieved in the simulation and the test to see the pressure differences.

A line was drawn in the CFD post against the axis of the cylinder and so the results in Excel files represent the data only at the drawn line (Appendix 2). This is done to replicate the position of piezoelectric blast wave pressure probes to measure the pressure of the blast wave. Table 10 shows the comparison between the experimental, literature simulation, and thesis simulation pressure values.

Table 10: Comparison of pressure results

Distances	Experimental pressure measurement (Zalosh and Weyandt 2005)	Pressure estimated by (Kim, Shentsov et al. 2017)	Pressure estimated in this study
1.9 m	300 kPa	300 kPa	307.79 kPa
4.2 m	83 kPa	<83 kPa	114.70 kPa
6.5 m	41 kPa	<40 kPa	58.75 kPa

4.2.2 Small-scale CGH2 Tank (Transversal axis)

The execution of the model for the tank transversal axis blast wave analysis is similar to the process adopted for simulating the tank longitudinal axis blast wave. Similarly, the results will be accompanied by pressure, temperature, and velocity profiles. The overpressure comparison was not presented due to the absence of the overpressures in literature followed for this axis.

4.2.2.1 Grid Independence Study

Table 11 shows the comparison of the three types of mesh used for the model and the results achieved on the respective mesh.

Table 11: Grid independence test comparison

Mesh Type	Elements	Pressure (kPa) at 1.5 e-3 s and 0.86 m from the tank	Temp (K) at 1.5 e-3 s and 0.86 m from the tank	Error (%) (pressure)	Error (%) (temperature)
Coarser	9440	425.69	214.40	-	-
Medium	24087	316.08	191.60	29.55	11.23
Fine	31729	321.33	194.91	1.65	1.71

Figure 13 shows the graphical demonstration of the grid independence test for the model.

The refinement ratio must be higher than 1.3, according to the Richardson extrapolation (Roache 1993).

Refinement ratio of fine and medium mesh $= \frac{\text{Fine mesh elements}}{\text{Medium mesh elements}} = 1.32$

Refinement ratio of medium and coarse mesh $= \frac{\text{Medium mesh elements}}{\text{Coarse mesh elements}} = 2.55$

The refinement ratio is acceptable to conduct analysis and the relative error reduces further as the mesh turns into a finer mesh.

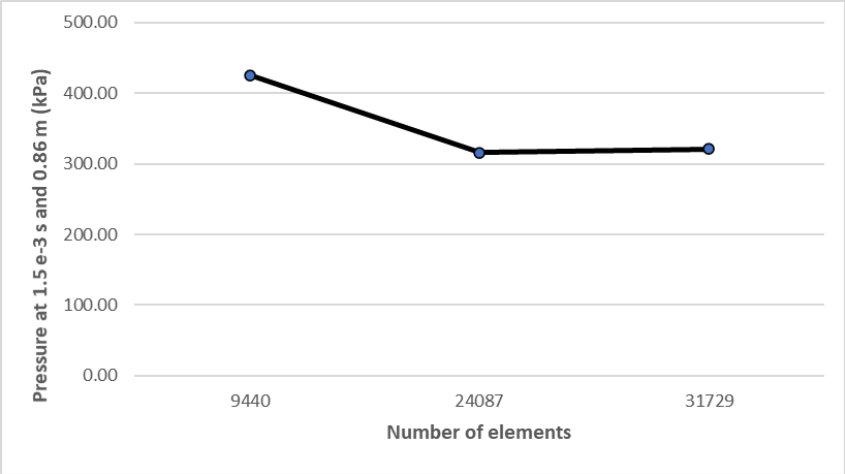

Figure 13: Grid independence test plot

4.2.2.2 Pressure profile

Figure 10 and 14 shows the propagation of the blast wave generated upon tank rupture both longitudinal and transverse to the tank axis. The behavior of blast wave is slightly distinct in comparison to blast wave propagation at the longitudinal axis. At 7e-4 s, the wave propagates out in the circular motion due to the cylindrical shape of the tank unlike longitudinally which was rather hemispherical. The highest overpressure effect which was observed at 9.7e-4 s at the longitudinal axis is lower on this axis 10.33 MPa. However, at the bottom of the tank, the pressure wave hits the ground and reflects upwards. At 3.3e-4 s, the reflecting wave forms a minute secondary wave effect as compared to in longitudinal axis analysis above. The wave shape adopts the circular shape and continues to expand. The higher-pressure region in this case stays near to the ground as compared to the top part throughout the propagation.

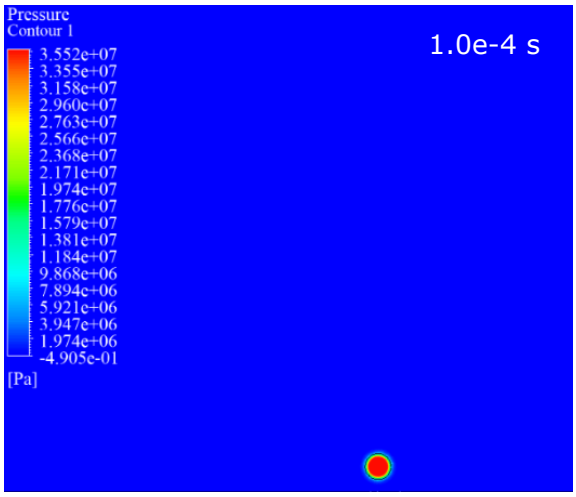

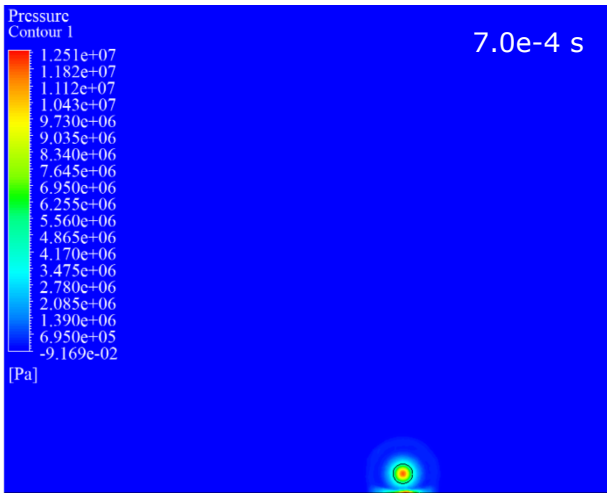

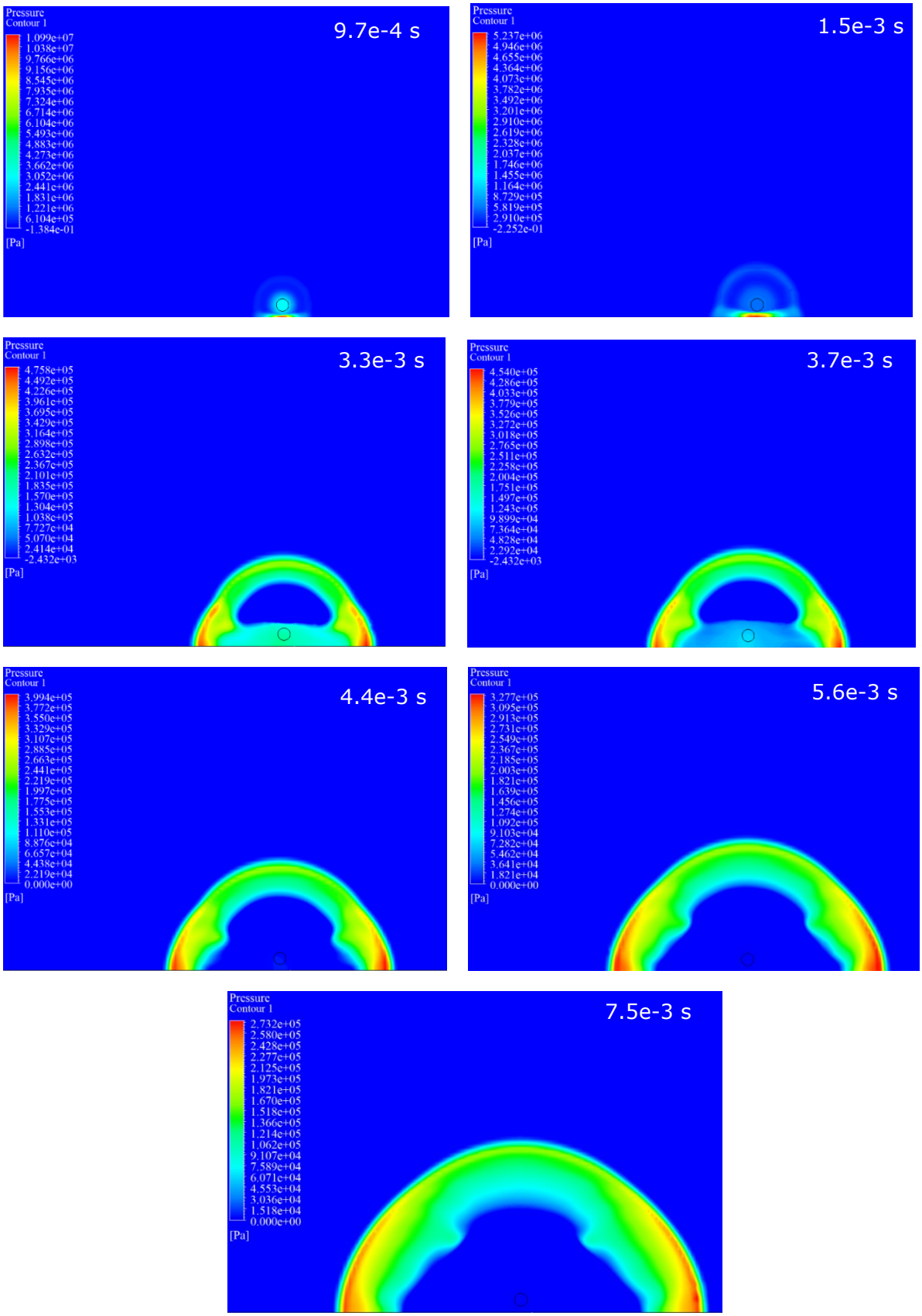

Figure 14: Pressure wave evolution at different time steps upon CGH2 rupture – Small-scale tank transversal axis

4.2.2.3 Temperature profile

Figure 15 represents the temperature profile of the blast wave propagated transversely to the tank axis. Similarly, on this axis, the temperature initially increases as the tank ruptures. There is a sudden rise in the temperature near the ground at 7.0e-4 sec, due to the compression of the surrounding air. The reduction in the temperature around the tank (the blue region) is where the hydrogen on instantaneous release expands. This is where the highest temperature is observed near the ground i.e., 595 K. With the time progression, the outer circular wave consists of high-temperature profiles as compared to the inner low-temperature region.

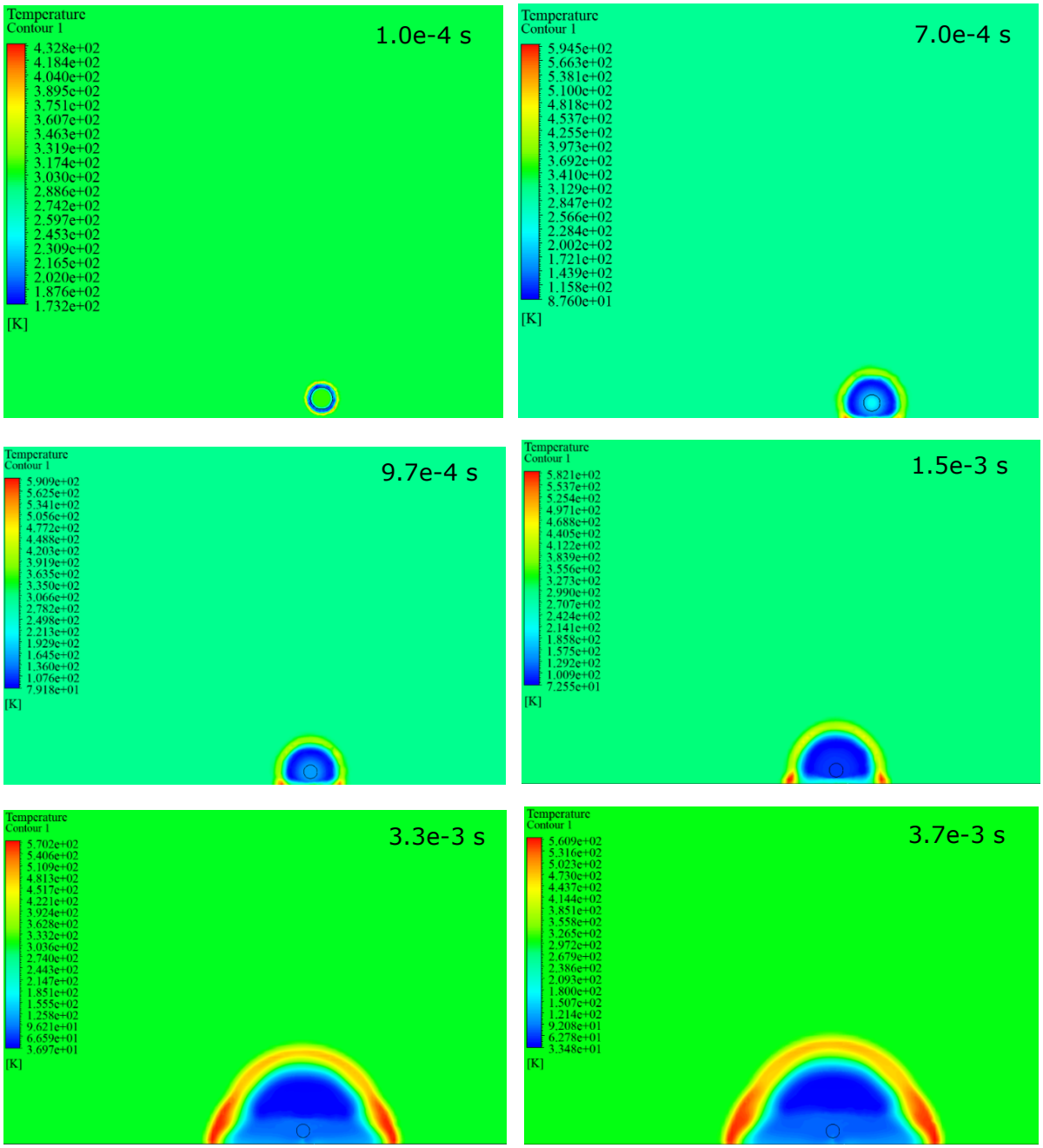

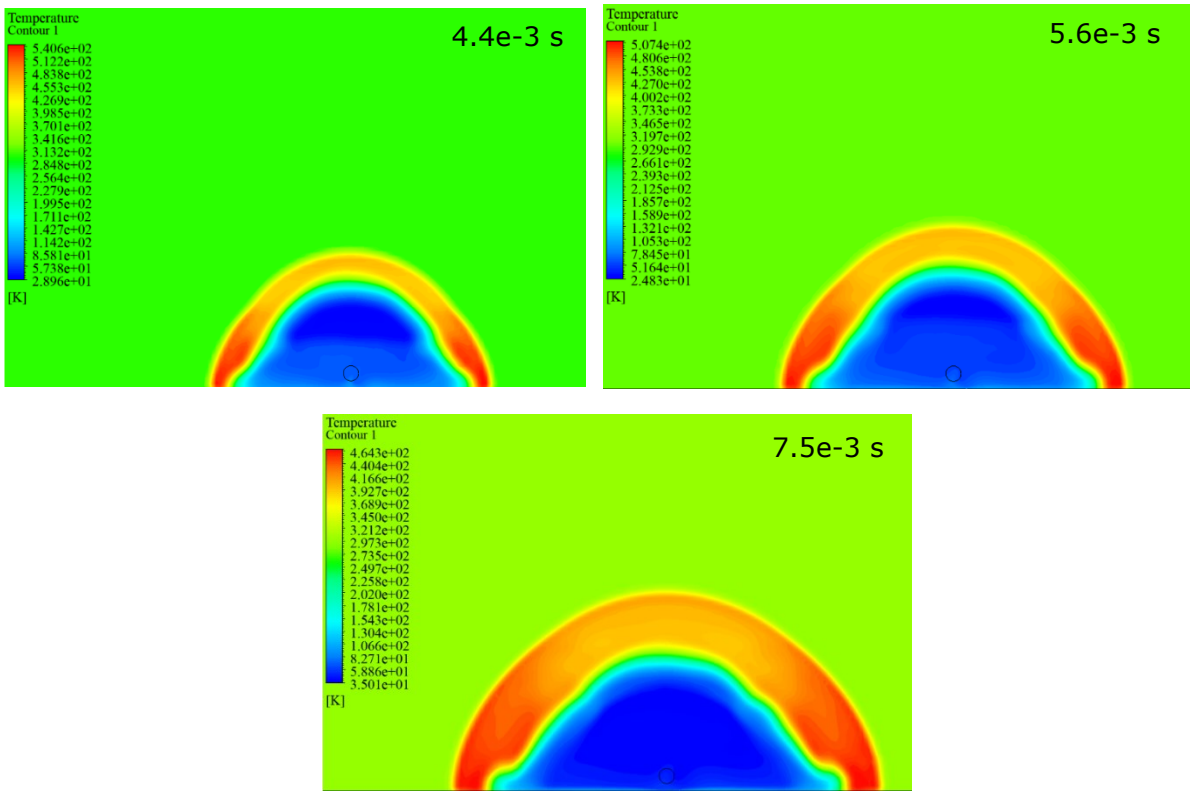

Figure 15: Temperature profile of the domain at different time steps – Small-scale tank transversal axis

4.2.2.4 Velocity profile

In figure 16, it can be seen that at 1.0e-4 s, the velocity is the highest 773 m/s the pressurized hydrogen releases instantaneously to the surroundings. Whereas, longitudinally to the tank the velocity was 826 m/s. As the wave propagates the velocity decreases and mostly stays around the tank in the circular motion. After 4.4e-4 sec the velocity around the tank and near the ground stays high. In later, steps the velocity of the wave is higher near the ground. Whereas longitudinally the velocity of the wave rises quite higher and along with the formation of secondary wave shows to high-velocity regions rising.

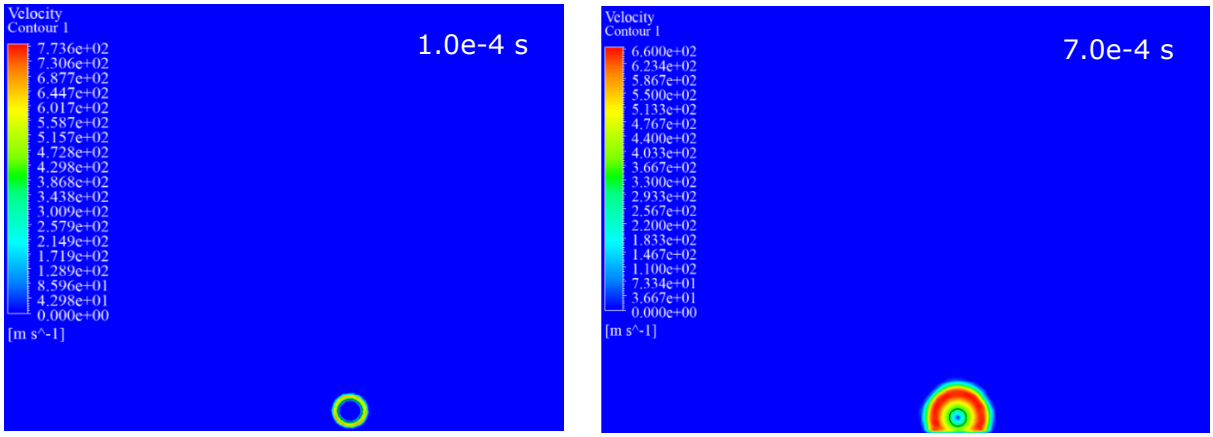

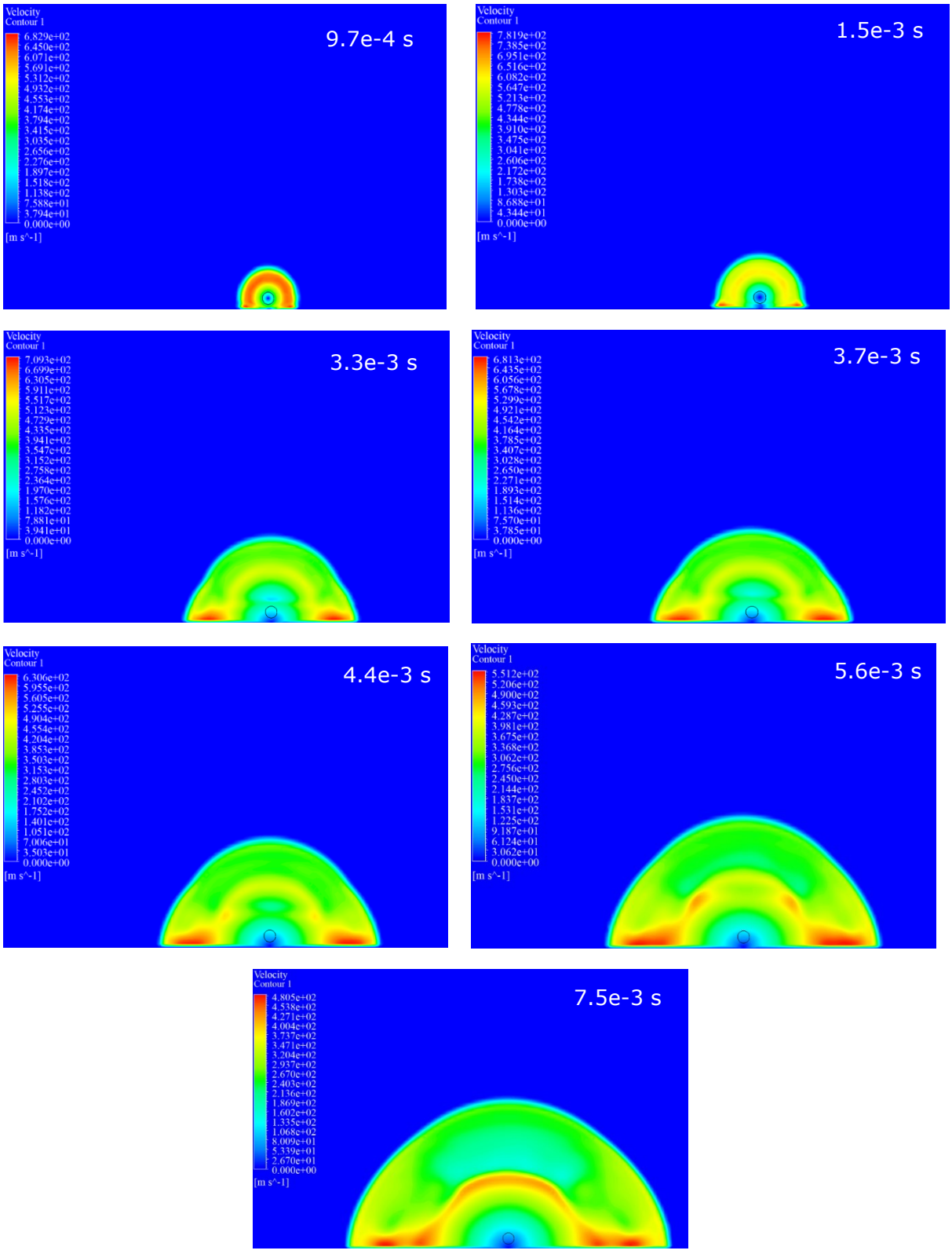

Figure 16: Velocity profile of the domain at different time steps – Small-scale tank transversal axis

4.2.3 Large-scale CGH2 Tank (Longitudinal axis)

4.2.3.1 Grid Independence Study

Table 12 shows the comparison of the three types of mesh used for the model and the results achieved on the respective mesh.

Table 12: Grid independence test comparison

Mesh Type	Elements	Pressure (kPa) at 7.5e-3 s and 1.04m from the tank	Temp (K) at 7.5e-3 s and 1.04m from the tank	Error (%) (pressure)	Error (%) (temperature)
Coarser	42642	276.99	105.70	-	-
Medium	103886	242.46	116.47	13.29	9.69
Fine	136926	242.98	117.87	0.21	1.19

Figure 17 shows the graphical demonstration of the grid independence test for the model.

The refinement ratio must be higher than 1.3, according to the Richardson extrapolation (Roache 1993).

Refinement ratio of fine and medium mesh $= \frac{\text{Fine mesh elements}}{\text{Medium mesh elements}} = 1.31$

Refinement ratio of medium and coarse mesh $= \frac{\text{Medium mesh elements}}{\text{Coarse mesh elements}} = 2.43$

The refinement ratio is acceptable to conduct analysis and the relative error reduces further as the mesh turns into a finer mesh.

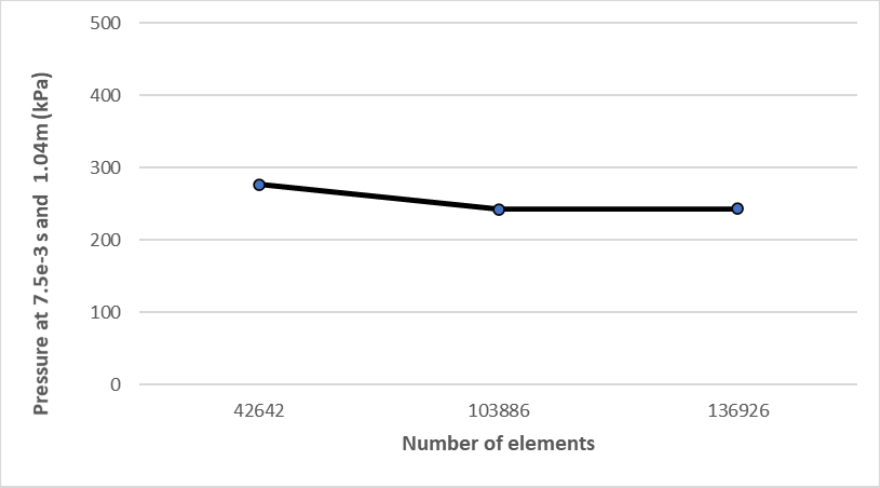

Figure 17: Grid independence test plot

4.2.3.2 Pressure profile

Figure 18 depicts the pressure profile of the blast wave propagation upon the rupture of the CGH2 tank along the longitudinal axis. The rupture as assumed initiates with the complete and instantaneous destruction of the tank walls. The depressurization begins immediately, at 4.0e-3 s the wave propagation to the surrounding and the high-pressure

region of 7.9 MPa under the tank is visible. The formation of the secondary wave initiates and rises upwards joining the first blast wave. At 7.5e-3 s, the wave shape becomes hemispherical with the effects of the secondary wave rising and expanding more near the ground perpendicular to the axis of the tank. In the middle portion of the tank, the high-pressure region retains longer and moves upwards forming a long tower-like region. It can be seen at 2.5e-2 s and 4.1e-2 s the secondary wave joins the first wave and generates more pressure toward the top region. However, the regions near the ground on both sides comprise relatively low-pressure regions, less than 100 KPa.

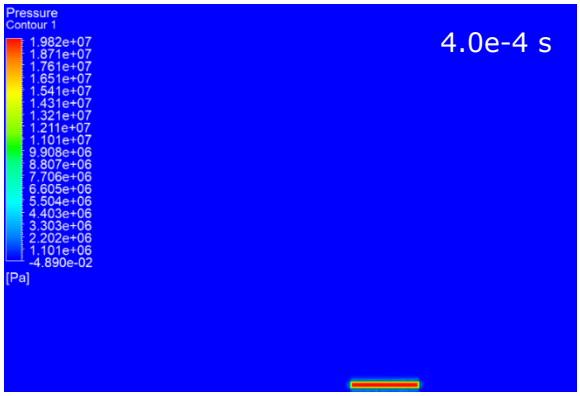

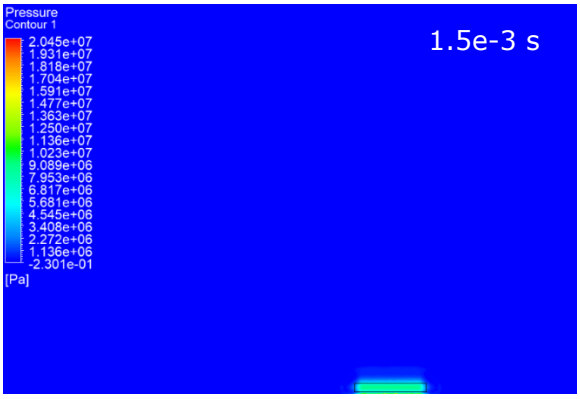

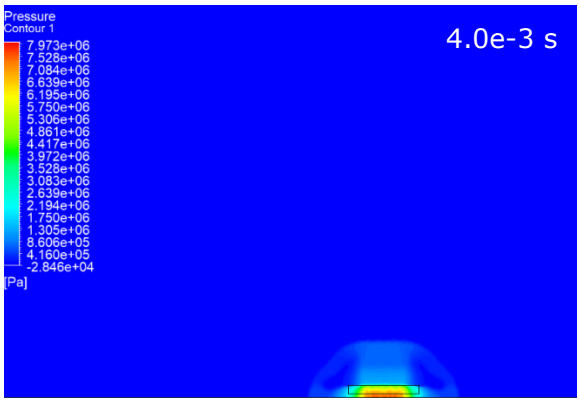

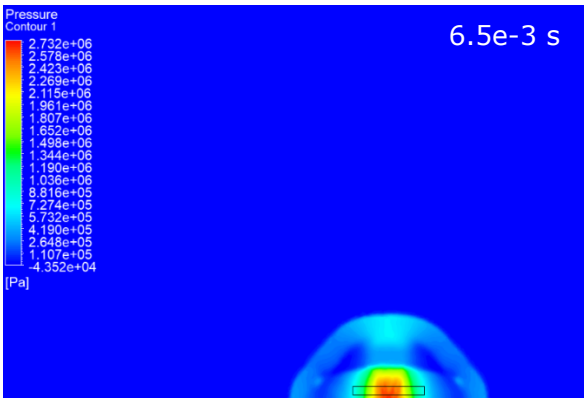

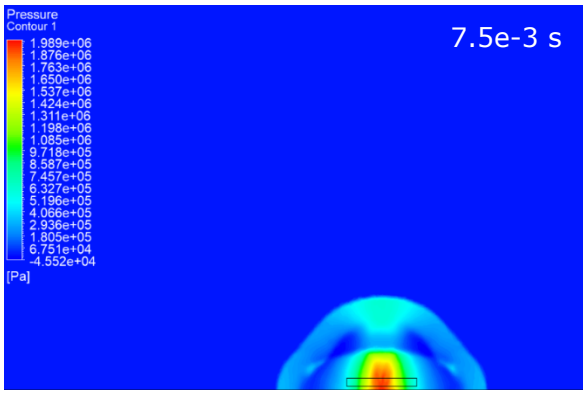

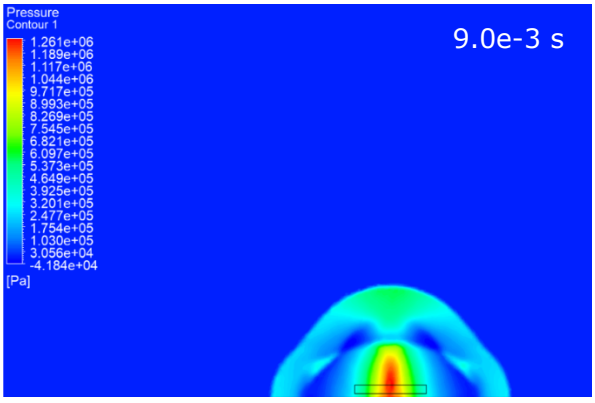

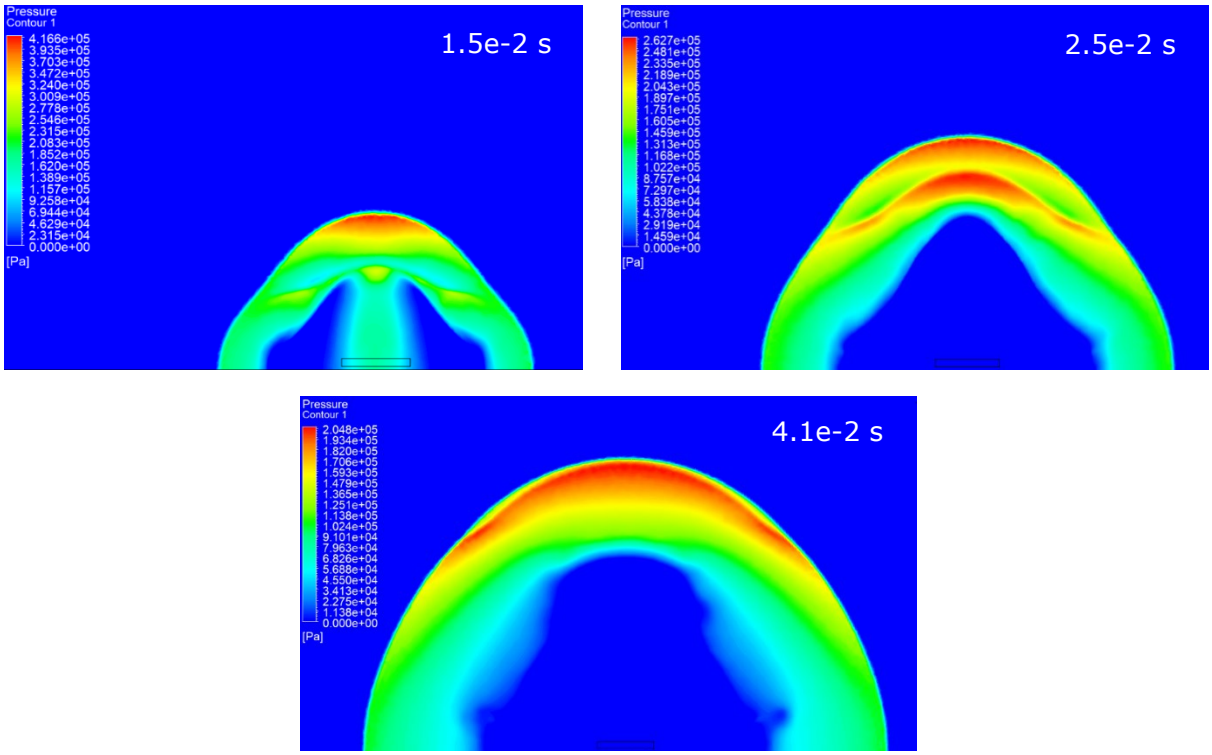

Figure 18: Pressure profile of the blast wave at different time steps – Large-scale tank (longitudinal axis)

Figure 19 shows the overpressures generated at several distances along the longitudinal axis of the tank 0.65m above the ground (the axis above 0.65 m shown in appendix 2).

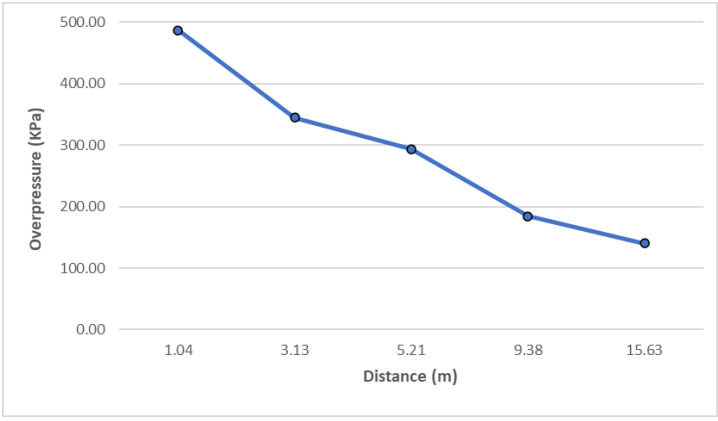

Figure 19: Maximum overpressure of the blast wave along the longitudinal axis

4.2.3.3 Temperature profile

Figure 20 shows the temperature profile of the blast wave following the same time intervals as shown in figure 19. At the initiation of the rupture the temperature around the tank region is around 541 K. At 4.0e-3 s, due to the sudden expansion the temperature in the surroundings begins to increase to 671 K the highest observed, the sudden temperature increase is due to the compression of air. On other hand, the regions near the tank show

low temperatures because of hydrogen expansion. With the time progression, the outer hemispherical wave consists of high-temperature profiles as compared to the inside low-temperature region.

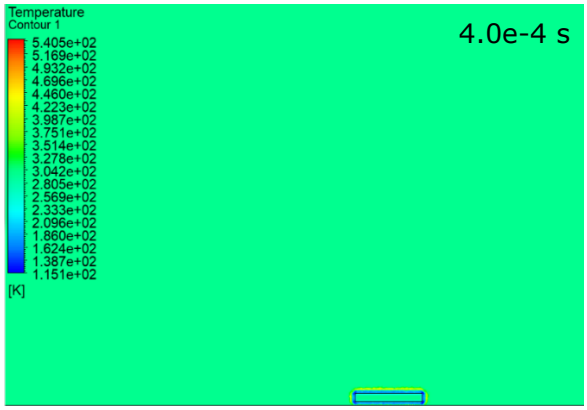

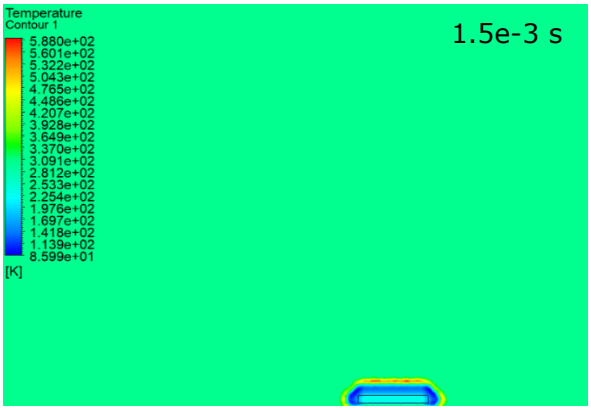

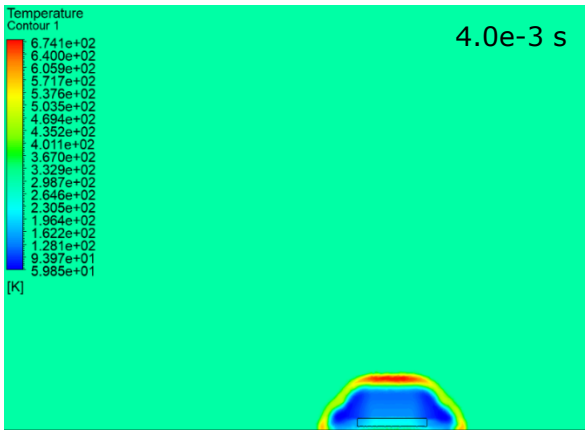

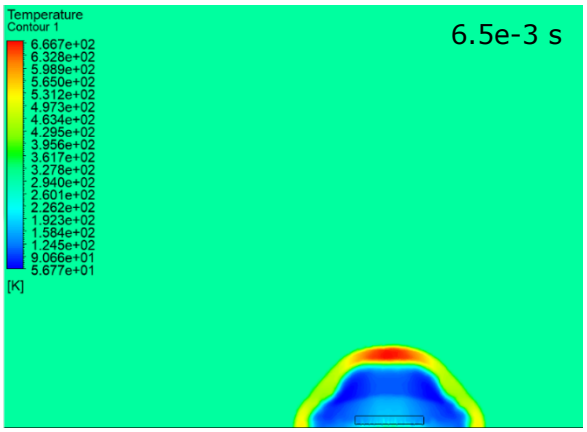

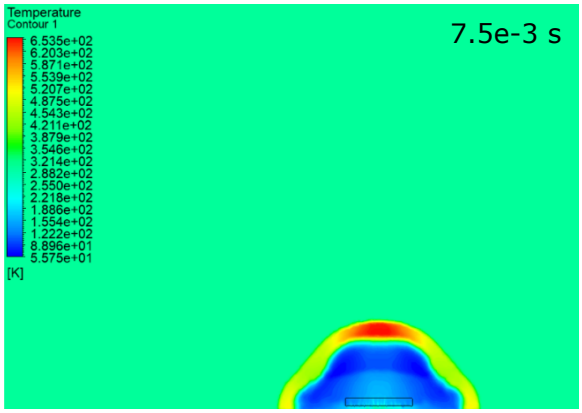

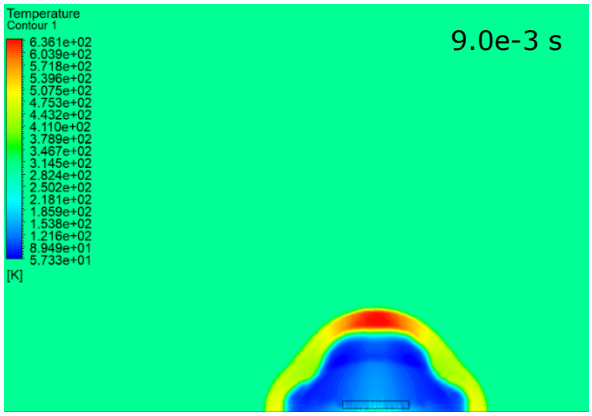

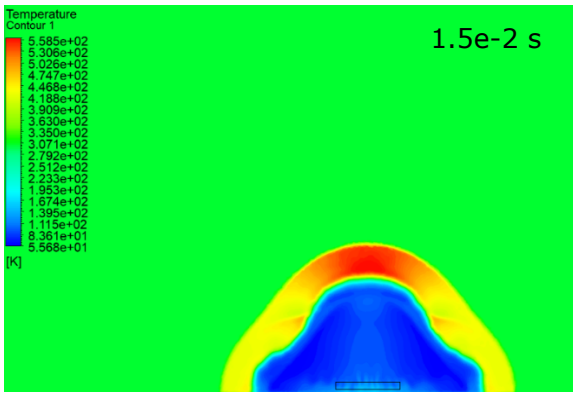

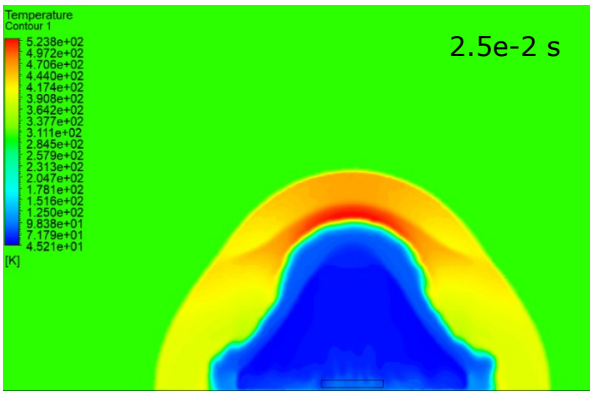

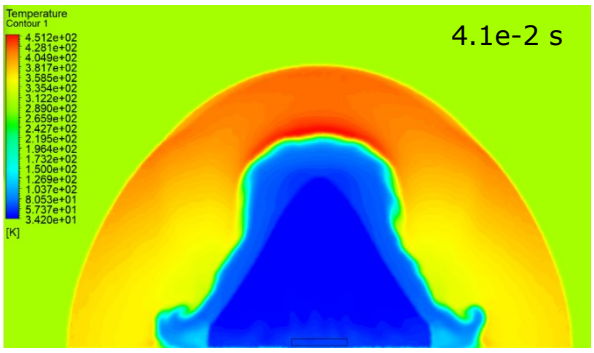

Figure 20: Temperature profile of the domain at different time steps – Large-scale tank (longitudinal axis)

4.2.3.4 Velocity profile

Figure 21 shows the velocity profile of the blast wave propagated. The velocity at 4.0e-4 s is the highest 694 m/s and with the time the top part of the tank shows a high-velocity region. With the formation of the secondary waves due to reflection on the ground, at 4.0e-3 s, the velocity regions are higher near the ground and the top of the tank: 576 m/s and 653 m/s, respectively. With time the wave propagates, and the velocity of the blast can be seen decreasing with time. However, at 2.5e-2 s the secondary blast wave joining with the first wave is visible and forms a high-velocity region of 520 m/s.

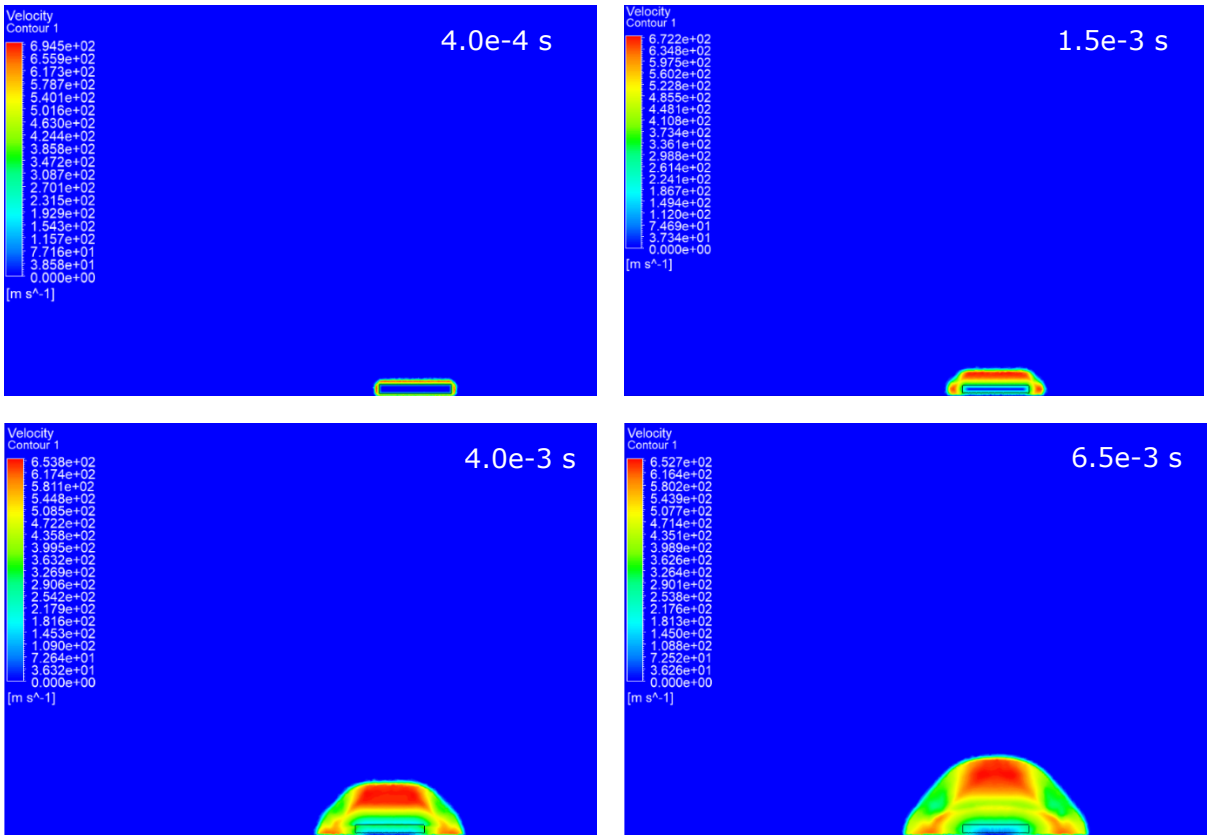

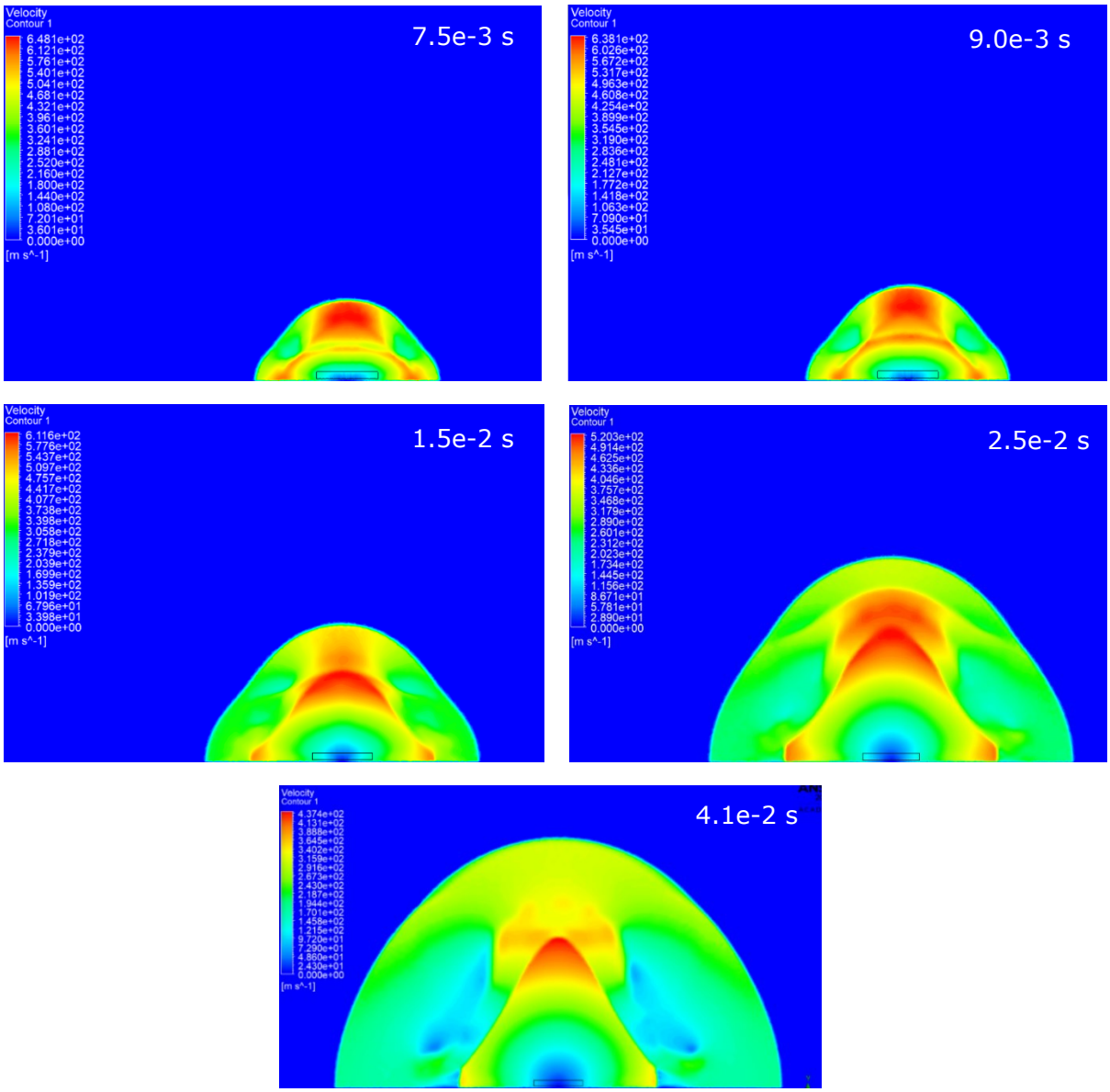

Figure 21: Velocity profile of the domain at different time steps – Large-scale tank (longitudinal axis)

4.2.4 Large-scale CGH2 Tank (Transversal axis)

The execution of the model for the tank transversal axis blast wave analysis is similar to the process adopted for simulating the tank longitudinal axis blast wave. Similarly, the results will be accompanied by pressure, temperature, and velocity profiles.

4.2.4.1 Grid Independence Study

Table 13 shows the comparison of the three types of mesh used for the model and the results achieved on the respective mesh.

Table 13: Grid independence test comparison

Mesh Type	Elements	Pressure (kPa) 1.5e-3 s and 0.50m from the tank	Temp (K) at 1.5e-3 s and 0.50m from the tank	Error (%) (pressure)	Error (%) (temperature)
Coarser	64527	301.46	101.84	-	-
Medium	134714	253.67	93.50	17.21	8.54
Fine	188712	249.69	92.1	1.58	1.49

Figure 22 shows the graphical demonstration of the grid independence test for the model.

The refinement ratio must be higher than 1.3, according to the Richardson extrapolation (Roache 1993).

Refinement ratio of fine and medium mesh $= \frac{\text{Fine mesh elements}}{\text{Medium mesh elements}} = 1.40$

Refinement ratio of medium and coarse mesh $= \frac{\text{Medium mesh elements}}{\text{Coarse mesh elements}} = 2.09$

The refinement ratio is acceptable to conduct analysis and the relative error reduces further as the mesh turns into a finer mesh.

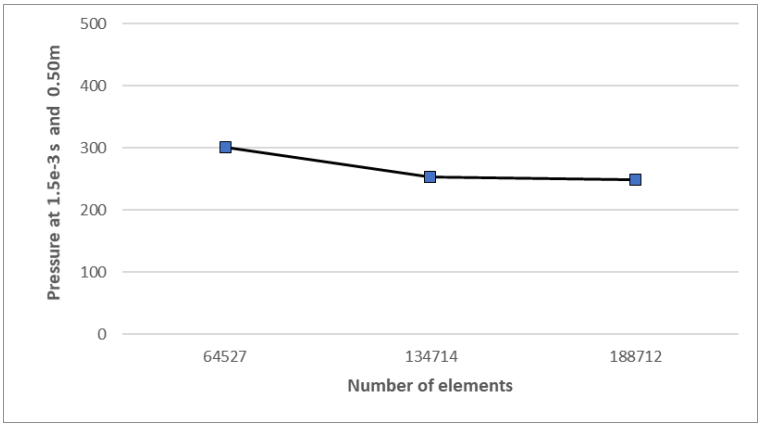

Figure 22: Grid independence test plot

4.2.4.2 Pressure profile

Figure 23 represents the pressure profile of the blast wave propagation on the transversal axis of the CGH2 tank upon rupture. The depressurization effect is immediately in effect, at 1.5e-3 s the wave propagation to the surrounding in a circular manner and impacts the ground. The formation of the secondary wave initiates and rises upwards joining the first blast wave. At 4.0e-3 s, the wave shape is more hemispherical with the effects of the secondary wave rising and expanding more near the ground perpendicular to the axis of the tank. At 7.5e-3 s and 9.0e-3 s, the pressure is higher near the ground rather than on the top of the wave in the case of longitudinal axis 289 and 255 KPa, respectively. However,

at 2.00e-2 s the regions near to the ground on both sides comprises relatively low-pressure regions approximately 100 KPa.

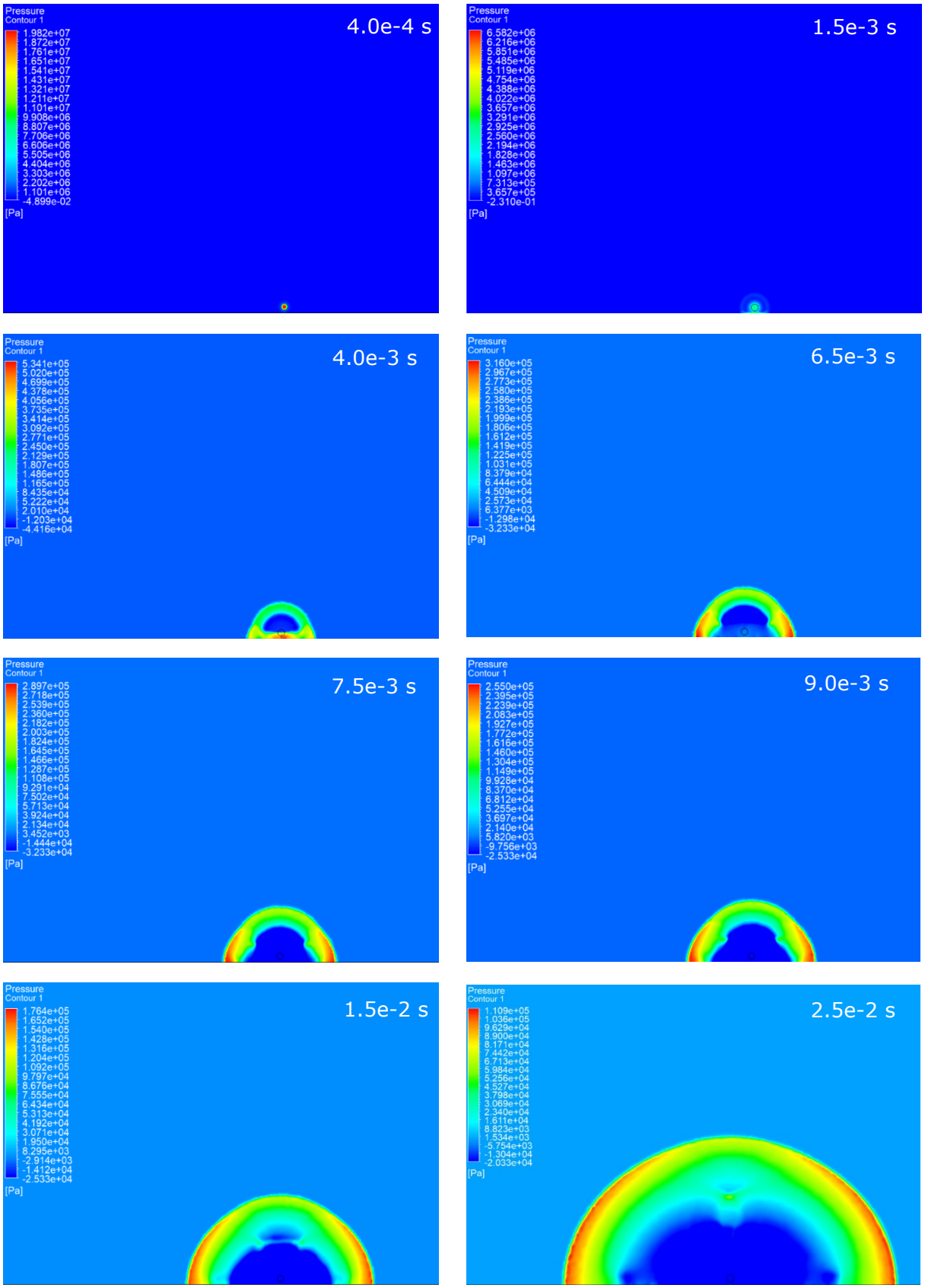

Figure 23: Pressure profile of the blast wave at different time steps – Large-scale tank (transversal axis)

Figure 24 shows the overpressures generated at several distances along the transversal axis of the tank 0.65m above the ground (the axis above 0.65m shown in appendix 2).

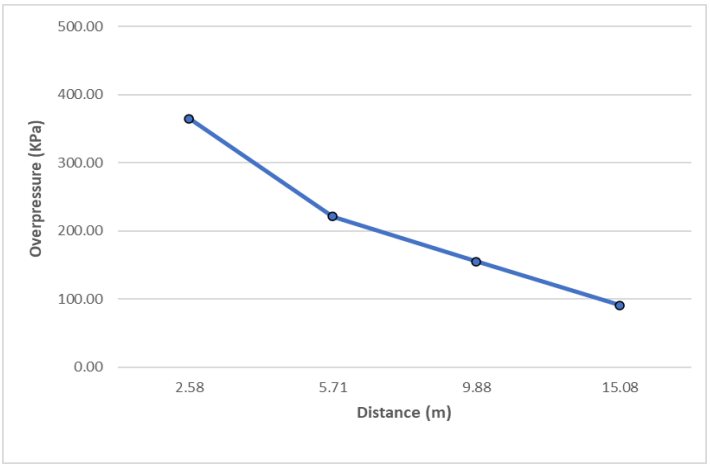

Figure 24: Maximum overpressure of the blast wave along the transversal axis at different distances

4.2.4.3 Temperature profile

Figure 25 represents the temperature profile of the blast wave propagated transversely to the tank axis. Similarly, on this axis, the temperature initially increases as the tank ruptures. There is a sudden rise in the temperature near the ground at 1.5e-3 sec, due to the compression of the surrounding air. The reduction in the temperature around the tank (the blue region) is where the hydrogen on instantaneous release expands. This is where the highest temperature is observed near the ground i.e., 573 K. With the time progression, the outer circular wave consists of high-temperature profiles as compared to the inner low-temperature region.

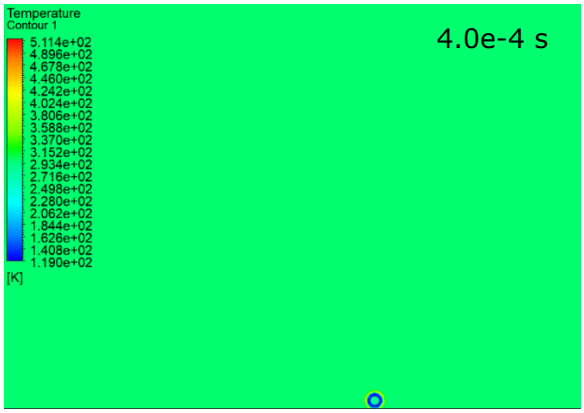

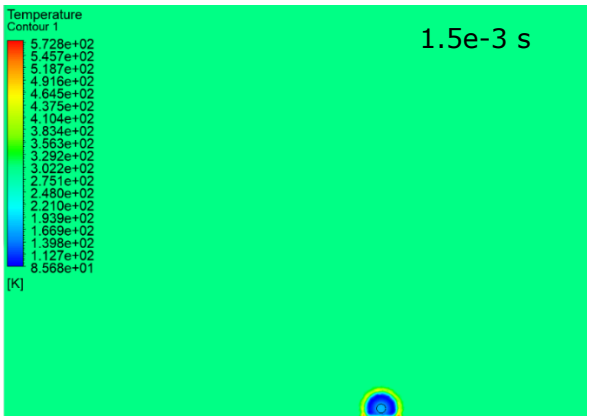

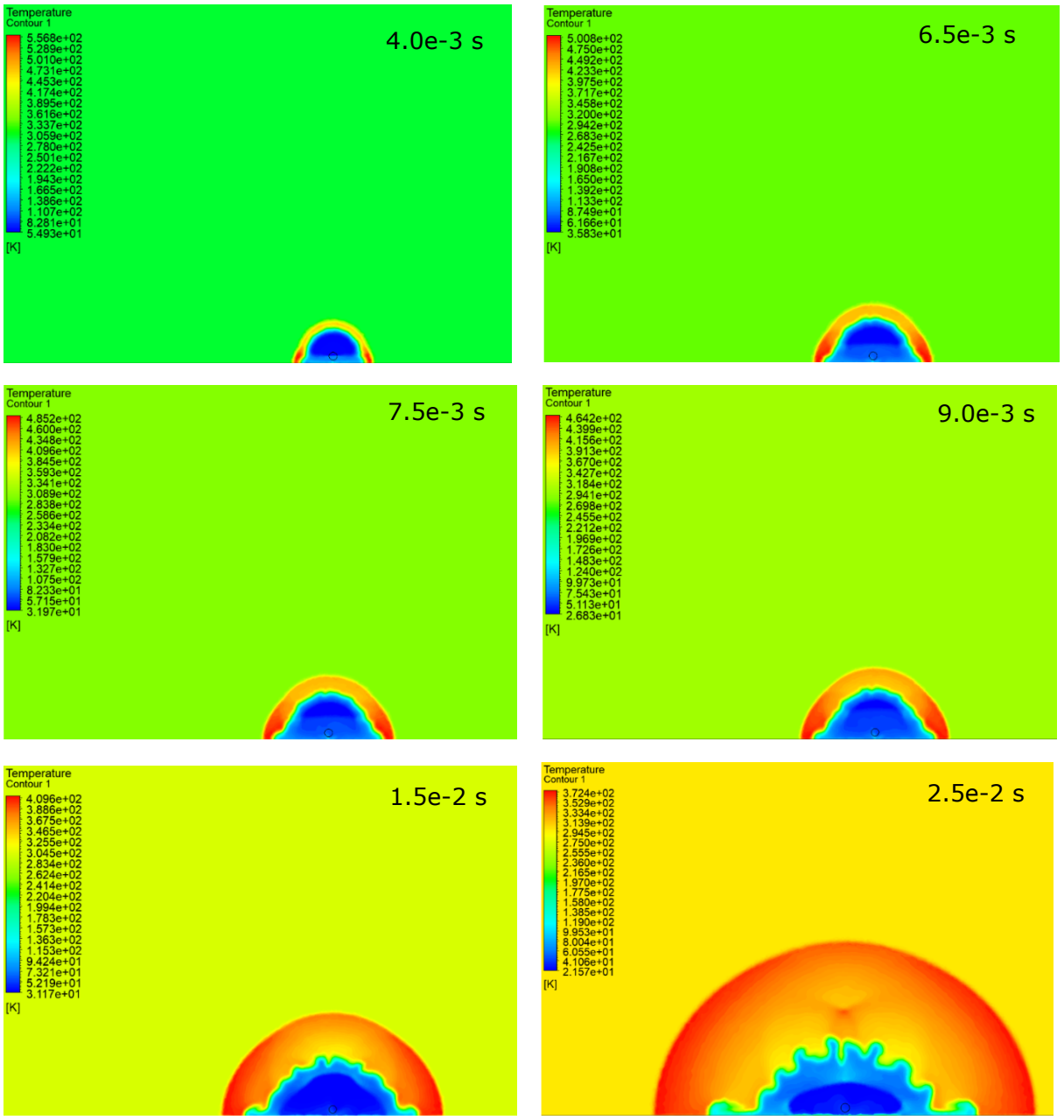

Figure 25: Temperature profile of the domain at different time steps – Large-scale tank (transversal axis)

4.2.4.4 Velocity profile

Figure 26 shows the velocity profile of the blast wave propagated. The velocity at 4.0e-4 s is 645 m/s and with time the top part of the tank shows a high-velocity region. With the formation of the secondary waves due to reflection on the ground, at 4.0e-3 s the velocity regions are higher near to the ground is the highest at 671 m/s. The wave continues to propagate circularly, and the velocity of the blast can be seen decreasing with time while remaining highest near to the ground. However, at 1.5e-2 s the secondary blast wave joining with the first wave is visible and reaches a value of 404 m/s. Whereas longitudinally the velocity of the wave rises quite higher and along with the formation of secondary wave shows to high-velocity regions rising.

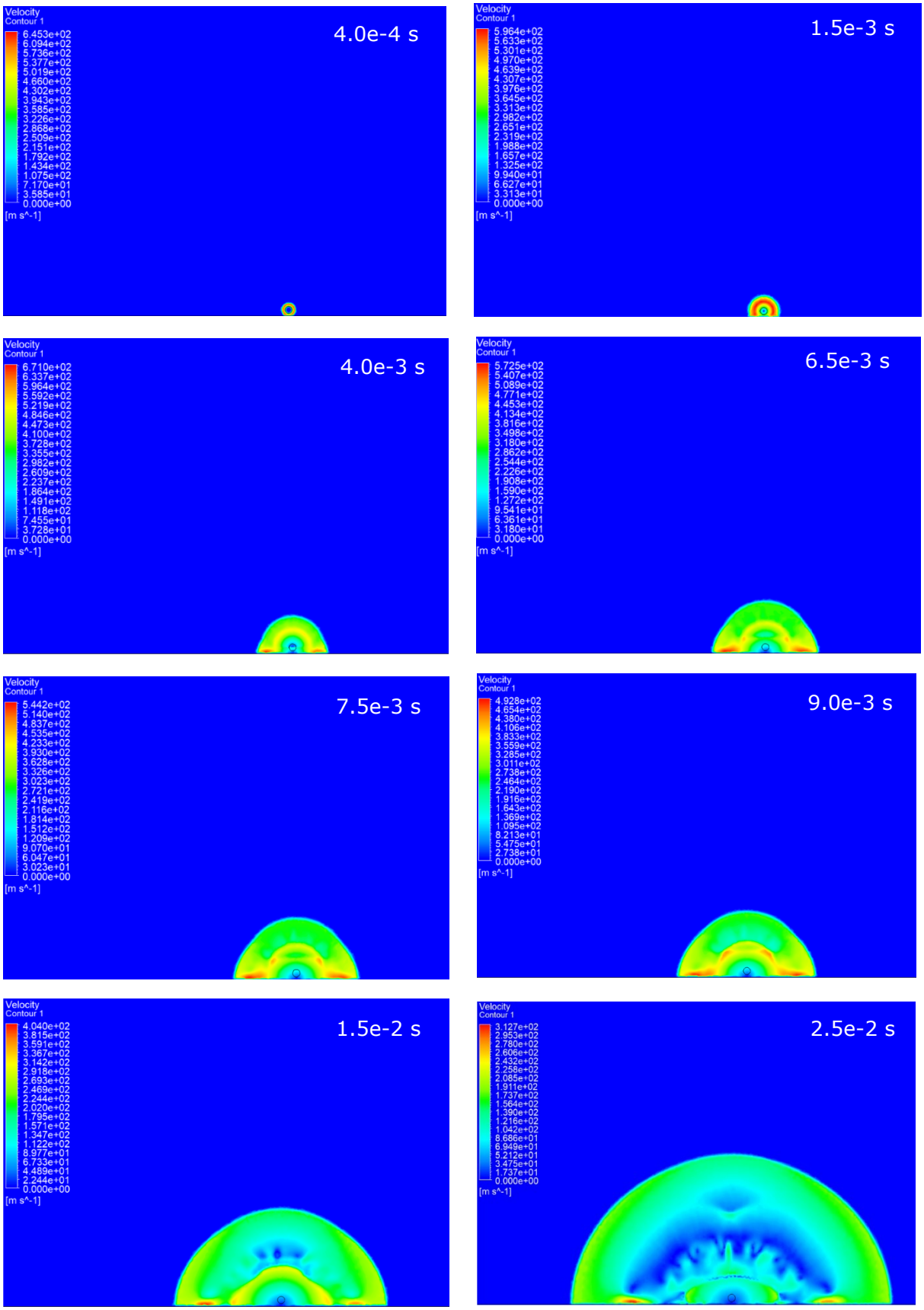

Figure 26: Velocity profile of the domain at different time steps – Large-scale tank (transversal axis)

4.2.5 Risk estimation

To calculate the risk of the fatality for the tank rupture scenario, the hazard distances for the blast wave from CFD conducted are utilized and tank rupture frequencies from literature are utilized. First using equation (2) from section 3.3.1, to determine the number of fatalities involved during the blast wave propagation on large-scale CGH2 tank rupture. Table 14 shows the blast wave distance covered having pressures >100 kPa along both axes.

Table 14: Blast wave hazard distances

Hazard Zone	**Blast wave distance (m)**	**Blast wave area (m^2)**
Fatality Zone (>100 kPa) Large-scale CGH2 tank – longitudinal axis	15.63	767.48
Fatality Zone (>100 kPa) Large-scale CGH2 tank – transversal axis	9.88	306.66

Now, for N_0 the location of the accident is considered as the extensively urbanized area of Norway from (Moilanen 2010) giving the population density of 0.000014 (person/m^2) and also assuming that there are 1.5 persons in the vehicle (Dadashzadeh, Kashkarov et al. 2018). Consequently, the number of fatalities expected during the large-scale CGH2 tank rupture is calculated as:

$N = N_0 \times A_{effect}$

$N = ((0.000014 \times 767.48) + (0.000014 \times 306.66)) + 1.5$

$= 1.514$ fatality/tank rupture consequence

In order to estimate the risk of the fatalities, the rupture frequencies are adopted from (Dadashzadeh, Kashkarov et al. 2018) which depicts the statistical data and calculated frequencies for the events leading to tank rupture. However, the data showed is assumed the frequencies of initiating tank rupture events to be equal to the traditional cars. The reason being the data related to the hydrogen vehicles is lower in comparison to traditional fuel vehicles which leads to very low frequencies of the initiating events for CGH2 tank rupture when determining fatalities risk. Table 15 shows the frequencies of the initiating events for tank rupture present in the literature.

Table 15: Frequencies of tank rupture initiating events.

Frequency of the initiating events leading to tank rupture	**rupture/vehicle/ year**
Frequency of initiating event due to car accident (Dadashzadeh, Kashkarov et al. 2018)	3.89e-5
Frequency of initiating event due to hydrogen filling/tow away (Saw, Flauw et al. 2016)	1.00e-6

Using the frequencies data, the total tank rupture frequency can be calculated as:

Total rupture frequencies = 3.99e-5 rupture/vehicle/year

Due to tank rupture, the risk of fatality per vehicle per year can be estimated using the equation (1):

$Risk_{fatality}$ = Rupture frequency x N = 3.99e-5 x 1.514 = 6.04e-5 fatality/vehicle/year

For the high-pressure tank ruptures the acceptable risk level is 1e-5 (LaChance, Houf et al. 2009), if compared to the risk estimated the risk is six times higher than the acceptable limit.

As there is a probability of the risk involved, the harm imposed to the human life due to the overpressures generated higher than 100 kPa as mentioned in section 3.3.1 is shown in table 16 below. The safe distance from the tank observed longitudinal to the large-scale tank is 23.96 m and transversal to the large-scale tank is 17.17m.

Table 16: Blast wave effect on people (Jeffries, Gould et al. 1996)

Effect on people exposed directly to the blast wave	**Pressure range (kPa)**
Instantaneous fatalities	482.6 - 1379
Lung haemorrhage - 90% probability	206.8 – 241.3
Lung haemorrhage - 50% probability	137.9 – 172.4
Eardrum rupture – 90% probability	68.9 – 103.4
Standing people fall due to pressure	55.2 – 110.3

Table 17 shows the summary of the results achieved for the blast wave propagation due to large-scale CGH2 tank rupture.

Table 17: Summary of large-scale CGH2 tank simulation results

	Tank rupture simulation results				**Risk estimation**
	Max pressure (kPa)	**Max temperature**	**Max Velocity**	**Safe distance**	
Longitudinal axis	486.65 at 1.04 m 344.60 at 3.31 m 293.36 at 5.21 m 184.48 at 9.38 m 140.43 at 15.63 m	671 K	694 m/s	23.96 m	6.04e-5 fatality/vehicle/year
Transversal axis	364.68 at 2.58 m 220.86 at 5.71 m 154.77 at 9.88 m 90.99 at 15.08 m	573 K	671 m/s	17.17 m	

5 Discussion

Hydrogen can be stored and transported in the compressed gaseous state at different pressures. The analysis gives a good overview of different types of CGH2 storages and the consequences involved during the handling of a storage system. It is evident from the properties of hydrogen that it is highly flammable thus imposing risk on the hydrogen storage systems. Similarly, the tendency of hydrogen to escape from a leak is higher than other gases due to its small molecular size. This might lead to uncontrollable dispersion in the environment. The effect of embrittlement on the integrity of the storage materials can result in the LOC of CGH2. The CGH2 are typically stored in type I, II, III, IV tanks. As specified in the thesis, the tanks vary in type of material, design, capacities, and intensity of risk involved. The type IV tank tends to carry a higher amount of hydrogen compared to other tank types thanks to the use of composites materials in the construction. To systematically structure and map the analysis of the consequence involved in the CGH2 storage tank, the bow-tie method has been employed. Within the CGH2 storage system, the critical events are rupture of the tank, a leak from the pipe or a hose, a breach on the tank shell (different size of holes), and the ignition of a fire. Similarly, a critical event leads to a specific consequence or several consequences such as gas dispersion or jet fire due to breach in tank shell, blast wave, or fireball generated by a catastrophic tank rupture with consequent explosion. In the thesis the critical event dealt with is the catastrophic rupture of the CGH2 tank and the consequence under analysis is the blast wave generation and propagation. The analysis of the consequence determines the behavior of the CGH2 expansion and generation of blast wave overpressures at certain distances.

The blast wave upon CGH2 tank rupture was analyzed, and two different sizes of tanks were considered: one small- and one large-scale CGH2 tanks. A total of four 2D simulations were developed, two representing the longitudinal and transversal axes of the small- and large-scale CGH2 tanks, respectively. Different assumptions were defined in the model. Firstly, the small-scale CGH2 tank, with an initial internal pressure of 34.6 MPa, length and diameter equal to 0.84 m and 0.41 m, respectively, was simulated. The highest overpressure of the blast wave was 25.86 MPa was observed at 9.7e-4 s near the ground for this tank. The results of pressures were compared with the experimental and literature results in table 10. In comparison, the difference between the achieved pressures and the experimental and literature results was smaller than 1.47 %. The reasons for the difference in the results could be due to the different configurations: domain shape, 2D simulation, and mesh quality. The highest temperature observed was 622 K at 1.5e-3 s near the ground due to the reflection of the pressure wave. The detonation effect with the velocity of 826 m/s was observed at 1.0e-4 s. While analyzing large-scale CGH2 tank a prominent difference was observed in the overall results. Along the longitudinal axis of the large-scale tank, the blast wave having pressures greater than 100 kPa propagates up to 15.63 m and safe distance observed at 23.96 m with pressure lower than 1.3 kPa. Similarly, along the transversal axis of the large-scale tank, the blast wave having pressures greater than 100 kPa propagates up to 9.88 m, and a safe distance observed at 17.17 m with pressure lower than 1.3 kPa. As expected, the safety distance is larger along the longitudinal axis of the tank. The highest temperature of 671 K was observed at 4.0e-3 s above the tank due to compression of air. The detonation effect with the velocity of 694 m/s was observed at 1.0e-4 s. The maximum velocity estimated in the domain of the large-size tank was lower

compared with the small-scale CGH2 tank domain. The reason for this could be due to the initial tank pressure which was 34.6 and 20 MPa in the small and large-scale CGH2 tanks, respectively. From the literature, it was noticed that the pressures above 100 kPa are fatal, and less than 1.3 kPa are safe for humans. The fatality risk calculated for the human presence within the vicinity of the tank during the explosion is found to be 6.04e-5 fatality/vehicle/year. The acceptable risk level for high-pressure tank ruptures is 1e-5, thus the risk estimated is six times higher than the acceptable limit. As a result, the CGH2 storage systems under study need to be safer by increasing the reliability of the equipment, use of safety instruments and equipment to prevent tank rupture. Additionally, layers of protection in the system to mitigate the tank destruction consequences can be adopted. For instance, a continuous wall between the truck drivers' cabin and the storage tank must be installed. The overall results of the two types of tanks analyzed showed a significant difference, as it can be expected from the tanks of different sizes, capacities, and operative conditions. This influenced the safety distance as well as the risk. Additionally, the validated CFD model developed can be utilized to conduct a detailed analysis of the CGH2 tank rupture consequences as a predictive tool.

As discussed with regards to safety, there is still a knowledge gap to fill and the overall risks involved while handling CGH2 storages must be evaluated. The CGH2 tank upper-pressure limit of 200 bar is common practice to transport large amounts of hydrogen in Norway. The tube trailers operating at this pressure can carry up to 600 kg of hydrogen identified by Hylaw (Hylaw 2020). Several factors are not specifically defined in ADR concerning pressure limits, weight limits, and preferred tank design and type. A trailer can carry up to 6,200 Nm^3 of hydrogen with storage pressure of 200 - 300 bar (EU 2019). Concerning the design of tanks, HEXAGON a technology group collaborated with Standard Norway to develop ISO standards for hydrogen (ISO 17519). Hexagon using ISO 17519 standards, has achieved 1,000 bar pressure in type III tanks. The vehicles used for transporting CGH2 are currently less in number compared to the vehicles transporting conventional fuels. If relying only on the accident data for vehicles transporting CGH2, the initiating events frequencies are very low. Currently, to estimate risk it can be assumed that the hazard initiating events frequency would be equal to those of conventional fuel vehicles.

6 Conclusion

This study pinpoints the causal events such as hydrogen embrittlement, vehicle accidents, storage system equipment failure that might result in the tank catastrophic rupture critical event. This critical event can lead to a blast wave propagation, generation of fireball, jet fire, gas jet, or gas dispersion depending on the environmental conditions and type of rupture. It is expected that the intensity of the risk depends on the type of consequences. In the thesis, a detailed consequence analysis of the blast wave propagation upon CGH2 tank catastrophic rupture was presented using Ansys Fluent. The results indicate that this accident scenario may lead to serious consequences. The analysis points out that the blast wave can propagate up to several meters and have the tendency to harm human life within its vicinity. The estimated blast wave overpressures can result in fatality, permanent damage to the human organs, and minor harm.

The validated CFD model generated can be used to conduct a full investigation of the CGH2 tank rupture consequences. Such models can contribute to defining hazard and safe distances for consequences in case of CGH2 tank rupture having a different design and storage parameters. The analysis in the thesis reflects that the results developed from the CFD model can contribute to developing risk mitigating strategies for hydrogen storage systems. The analysis provides a holistic view to the MCE AS on the expected outcomes in case of the tank catastrophic rupture critical event when dealing with large-scale CGH2 tanks storage and transportation. Using CFD models, the company can make effective decisions when designing the transportation trucks and employing additional safety barriers to improve safety and reliability. The analysis highlights that there are several directions for further work and the following recommendations are provided:

- Consequence analysis of the fireball generation due to tank rupture, evaluating the effect of combustion on the overpressures, radiations, and estimating hazard distances.
- Using the real gas equation in the model to compare the parameters of the blast wave with the ideal gas equation results.
- Introducing a bundle of large-scale tubes in the model geometry to analyze the effect on the blast wave propagation and fireball generation.

References

ADR (2017). "ADRBook." from https://adrbook.com/en/2017/TabloA/1049.

Ahluwalia, R. K., et al. (2010). "Technical assessment of cryo-compressed hydrogen storage tank systems for automotive applications." International Journal of Hydrogen Energy **35**(9): 4171-4184.

Alcock, J. L. (2001). Compilation of Existing Safety Data on Hydrogen and Comparative Fuels.

Armaroli, N. and V. Balzani (2011). "The hydrogen issue." ChemSusChem **4**(1): 21-36.

Chen, T.-P. (2010). Hydrogen delivey infrastructure option analysis, Nexant, Inc., 101 2nd St., San Fancisco, CA 94105.

Dadashzadeh, M., et al. (2018). "Risk assessment methodology for onboard hydrogen storage." International Journal of Hydrogen Energy **43**(12): 6462-6475.

Damman, S., et al. (2020). "Largescale hydrogen production in Norway-possible transition pathways towards 2050." SINTEF Rapport.

Das, L. (1990). "Hydrogen engines: a view of the past and a look into the future." International Journal of Hydrogen Energy **15**(6): 425-443.

De Dianous, V. and C. Fievez (2006). "ARAMIS project: A more explicit demonstration of risk control through the use of bow–tie diagrams and the evaluation of safety barrier performance." Journal of Hazardous Materials **130**(3): 220-233.

de Ruijter, A. and F. Guldenmund (2016). "The bowtie method: A review." Safety Science **88**: 211-218.

Delvosalle, C., et al. (2006). "ARAMIS project: A comprehensive methodology for the identification of reference accident scenarios in process industries." Journal of Hazardous Materials **130**(3): 200-219.

Dickel, R. (2020). "Blue hydrogen as an enabler of green hydrogen: the case of Germany."

Drive, U. (2017). Hydrogen Delivery Technical Team Roadmap July 2017.

EU, H. (2019). "Horizontal Position Paper Transport and Distribution of Compressed Hydrogen by Road Quantity and Pressure Limitations."

Galassi, M. C., et al. (2012). "CFD analysis of fast filling scenarios for 70 MPa hydrogen type IV tanks." International Journal of Hydrogen Energy **37**(8): 6886-6892.

Gandía, L. M., et al. (2013). Chapter 1 - Renewable Hydrogen Energy: An Overview. Renewable Hydrogen Technologies. L. M. Gandía, G. Arzamendi and P. M. Diéguez. Amsterdam, Elsevier**:** 1-17.

Gerboni, R. (2016). 11 - Introduction to hydrogen transportation. Compendium of Hydrogen Energy. R. B. Gupta, A. Basile and T. N. Veziroğlu, Woodhead Publishing**:** 283-299.

Hylaw (2020). "Quantity and Pressure limitation." Retrieved 15 August, 2020, from https://www.hylaw.eu/database/norway/transport-and-distribution-of-hydrogen/road-transport-in-cylinders-and-tube-trailers-bulk-gas-metal-hydride-bulk-liquid/quantity-and-pressure-limitation.

Jeffries, R., et al. (1996). Derivation of fatality probability functions for occupants of buildings subject to blast loads. Probabilistic Safety Assessment and Management'96, Springer**:** 669-675.

Kaplan, S. and B. J. Garrick (1981). "On the quantitative definition of risk." Risk analysis **1**(1): 11-27.

Kashkarov, S., et al. (2020). "Blast wave from a hydrogen tank rupture in a fire in the open: Hazard distance nomograms." International Journal of Hydrogen Energy **45**(3): 2429-2446.

Kim, J. W., et al. (2014). 1 - Key challenges in the development of an infrastructure for hydrogen production, delivery, storage and use. Advances in Hydrogen Production, Storage and Distribution. A. Basile and A. Iulianelli, Woodhead Publishing**:** 3-31.

Kim, W., et al. (2017). "Simulations of blast wave and fireball occurring due to rupture of high-pressure hydrogen tank." Safety **3**(2): 16.

Kumar, S. (2015). Clean hydrogen production methods, Springer.

LaChance, J., et al. (2009). "Analyses to support development of risk-informed separation distances for hydrogen codes and standards." Sandia Report SAND2009-0874: 54.

McWhorter, S. and G. Ordaz (2013). "Onboard Type IV Compressed Hydrogen Storage Systems-Current Performance and Cost." US Department of Energy, Washington, DC, DOE Program Record **13013**.

Moilanen, M. (2010). "Matching and settlement patterns: The case of Norway." Papers in Regional Science **89**(3): 607-623.

Molkov, V., et al. (2021). "Dynamics of blast wave and fireball after hydrogen tank rupture in a fire in the open atmosphere." International Journal of Hydrogen Energy **46**(5): 4644-4665.

Norwegian Ministry of Petroleum and Energy, N. m. o. C. a. E. (2020). "The Norwegian Government's hydrogen strategy towards a low emission society ".

Noussan, M., et al. (2021). "The Role of Green and Blue Hydrogen in the Energy Transition—A Technological and Geopolitical Perspective." Sustainability **13**(1): 298.

Ordin, P. (1997). "Safety Standard for Hydrogen and Hydrogen Systems: Guidelines for Hydrogen System Design, Materials Selection, Operations, Storage, and Transportation. Office of Safety and Mission Assurance." National Aeronautics and Space Administration, Washington DC.

Pant, K. and R. B. Gupta (2009). "Fundamentals and use of hydrogen as a fuel." Hydrogen fuel: production, transport, and storage: 3-32.

Popov, B. N., et al. (2018). Chapter 7 - Hydrogen Permeation and Hydrogen-Induced Cracking. Handbook of Environmental Degradation of Materials (Third Edition). M. Kutz, William Andrew Publishing**:** 133-162.

Probstein, R. F. and R. E. Hicks (2006). Synthetic fuels, Courier Corporation.

Renkel, M. F. and N. Lümmen (2018). "Supplying hydrogen vehicles and ferries in Western Norway with locally produced hydrogen from municipal solid waste." International Journal of Hydrogen Energy **43**(5): 2585-2600.

Roache, P. J. (1993). "A method for uniform reporting of grid refinement studies." ASME-PUBLICATIONS-FED **158**: 109-109.

Royle, M. and D. Willoughby (2009). "Releases of unignited liquid hydrogen: Prepared by the Health and Safety Laboratory for the Health and Safety Executive 2014."

Salvi, B. and K. Subramanian (2015). "Sustainable development of road transportation sector using hydrogen energy system." Renewable and Sustainable Energy Reviews **51**: 1132-1155.

Saw, J. L., et al. (2016). The EU FireComp Project and risk assessment of hydrogen composite storage applications using bow-tie analysis. Hazards 26, Edinburgh UK.

Sherif, S., et al. (1997). "Liquid hydrogen: potential, problems, and a proposed research program." International Journal of Hydrogen Energy **22**(7): 683-688.

Simbeck, D. and E. Chang (2002). "Hydrogen supply: cost estimate for hydrogen pathways–scoping analysis." National Renewable Energy Laboratory **71**.

Stetson, N. T., et al. (2016). 1 - Introduction to hydrogen storage. Compendium of Hydrogen Energy. R. B. Gupta, A. Basile and T. N. Veziroğlu, Woodhead Publishing**:** 3-25.

Stygar, M. and T. Brylewski (2013). "Towards a hydrogen economy in Poland." International Journal of Hydrogen Energy **38**(1): 1-9.

Sylvester, A., et al. (2013). "Beyond synthesis: Re-presenting heterogeneous research literature." Behaviour & Information Technology **32**(12): 1199-1215.

Ulleberg, Ø. and R. Hancke (2020). "Techno-economic calculations of small-scale hydrogen supply systems for zero emission transport in Norway." International Journal of Hydrogen Energy **45**(2): 1201-1211.

UMOE (2018). Datasheet: Hydrogen storage and transportation solutions.

Ustolin, F., et al. (2020). "Loss of integrity of hydrogen technologies: A critical review." International Journal of Hydrogen Energy **45**(43): 23809-23840.

Ustolin, F., et al. (2020). "Loss of integrity of hydrogen technologies: A critical review." International Journal of Hydrogen Energy.

Van Cappellen, L., et al. (2018). Feasibility Study Into Blue Hydrogen: Technical, Economic & Sustainability Analysis, CE Delft.

Varin, R. A. and Z. S. Wronski (2013). Chapter 13 - Progress in Hydrogen Storage in Complex Hydrides, Elsevier B.V**:** 293-332.

Wang, Z., et al. (2018). "Life cycle greenhouse gas assessment of hydrogen production via chemical looping combustion thermally coupled steam reforming." Journal of Cleaner Production **179**: 335-346.

Weyandt, N. (2005). "Analysis of Induced catastrophic failure of a 5000 psig type IV hydrogen cylinder." Southwest Research Institute report for the Motor Vehicle Fire Research Institute **1**(01.001).

White, C., et al. (2006). "The hydrogen-fueled internal combustion engine: a technical review." International Journal of Hydrogen Energy **31**(10): 1292-1305.

Wurster, R. (2016). 9 - Hydrogen safety: An overview. Compendium of Hydrogen Energy. M. Ball, A. Basile and T. N. Veziroğlu. Oxford, Woodhead Publishing**:** 195-213.

Yang, C. and J. Ogden (2007). "Determining the lowest-cost hydrogen delivery mode." International Journal of Hydrogen Energy **32**(2): 268-286.

Zalosh, R. and N. Weyandt (2005). "Hydrogen fuel tank fire exposure burst test." SAE transactions: 2338-2343.

Appendices

Appendix 1: Screenshot of Ansys Model (geometry and mesh)

Appendix 2: Data plotting line on Ansys CFD post

Appendix 3: Glossary of Terms

Appendix 1

Geometry: Small-scale CGH2 tank (Longitudinal axis)

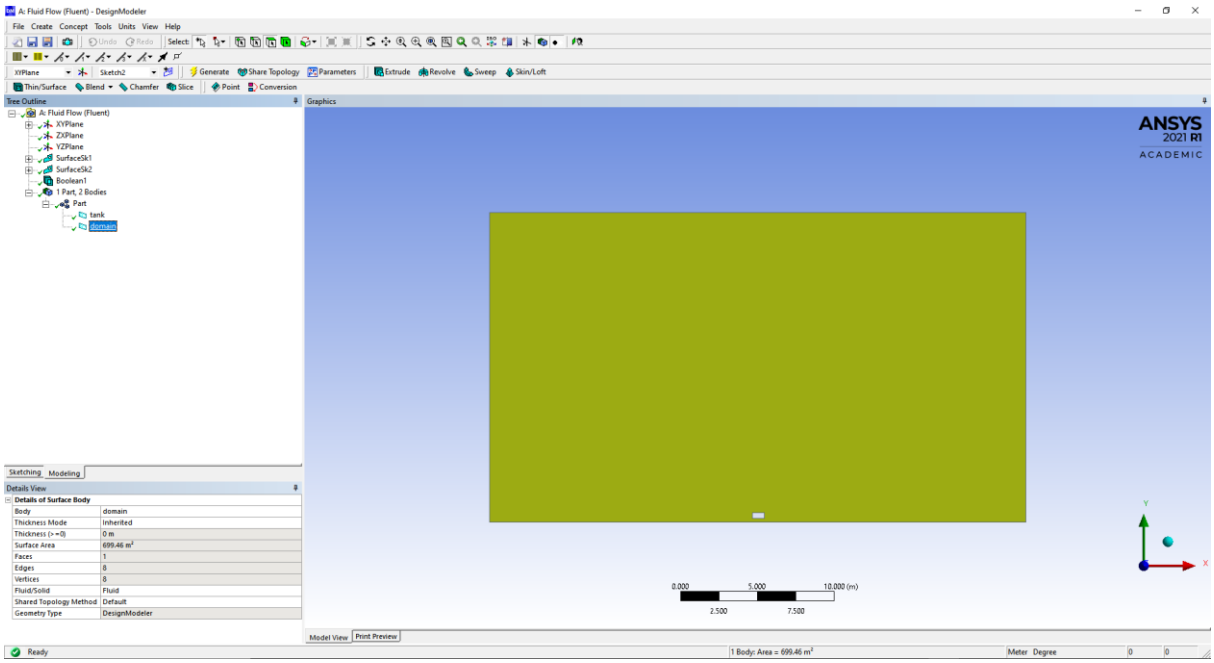

Geometry: Small-scale CGH2 tank (Transversal axis)

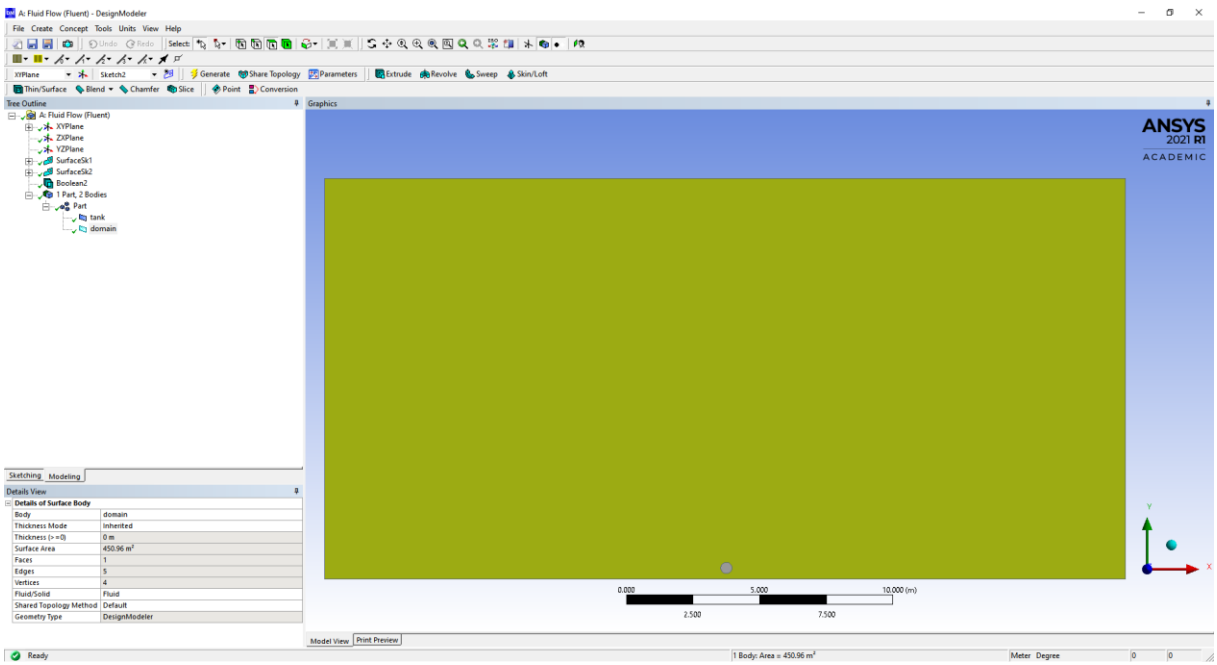

Geometry: Large-scale CGH2 tank (Longitudinal axis)

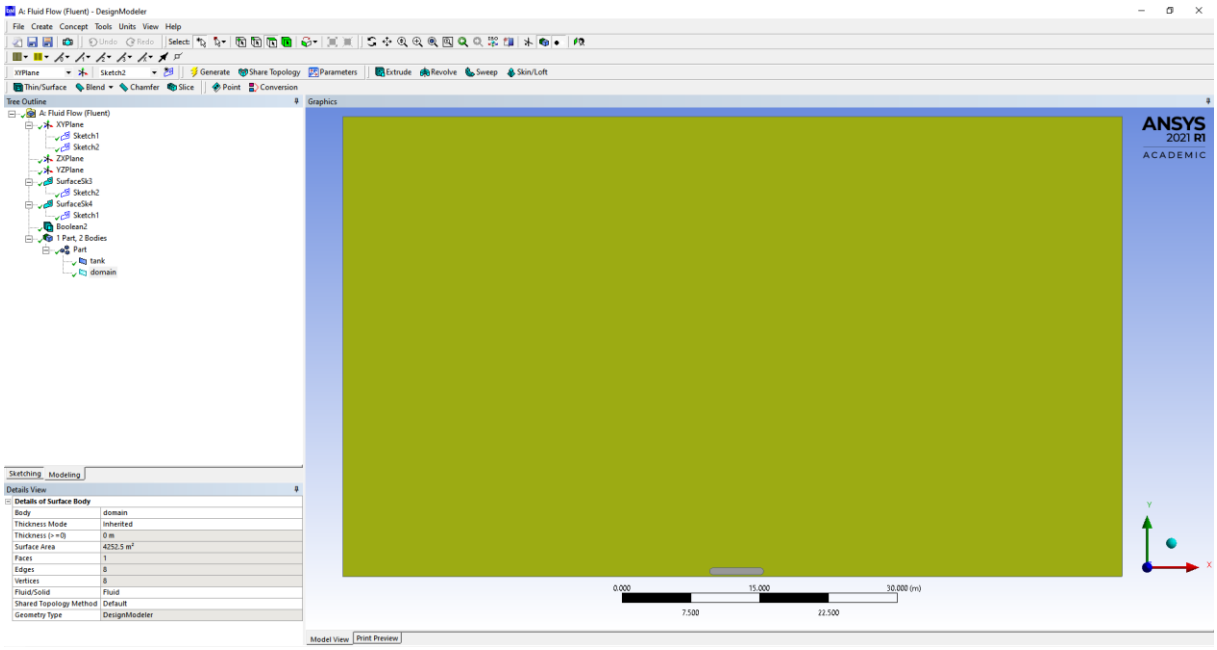

Geometry: Large-scale CGH2 tank (Transversal axis)

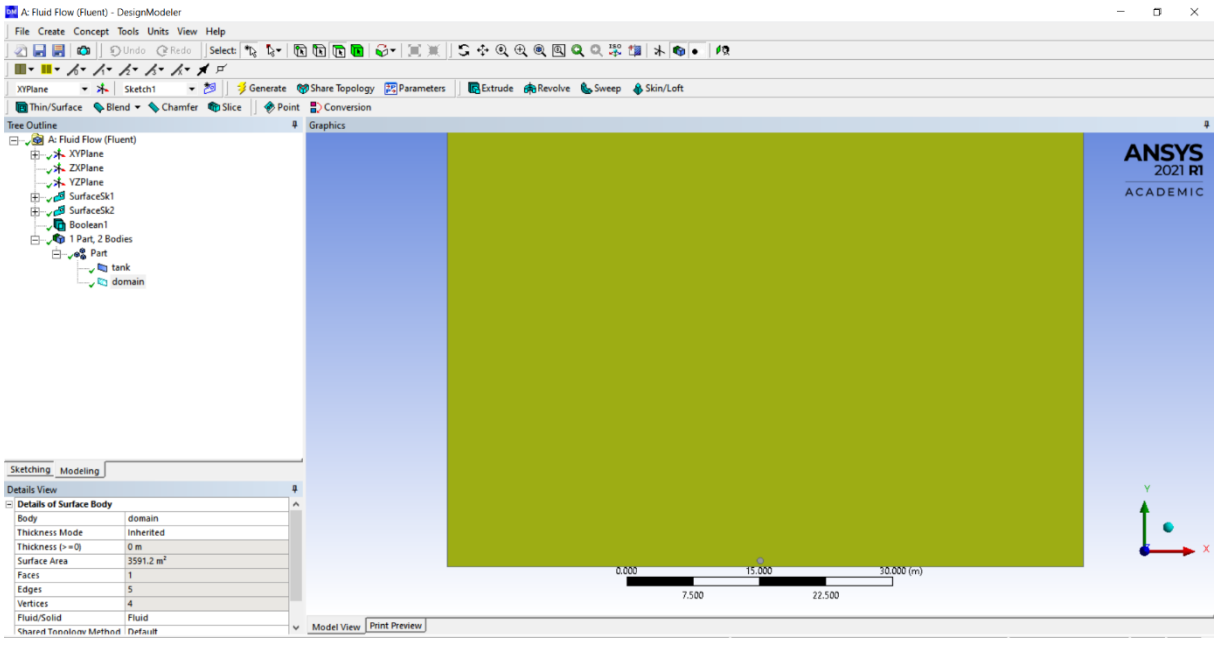

Mesh: Small-scale CGH2 tank (Longitudinal axis)

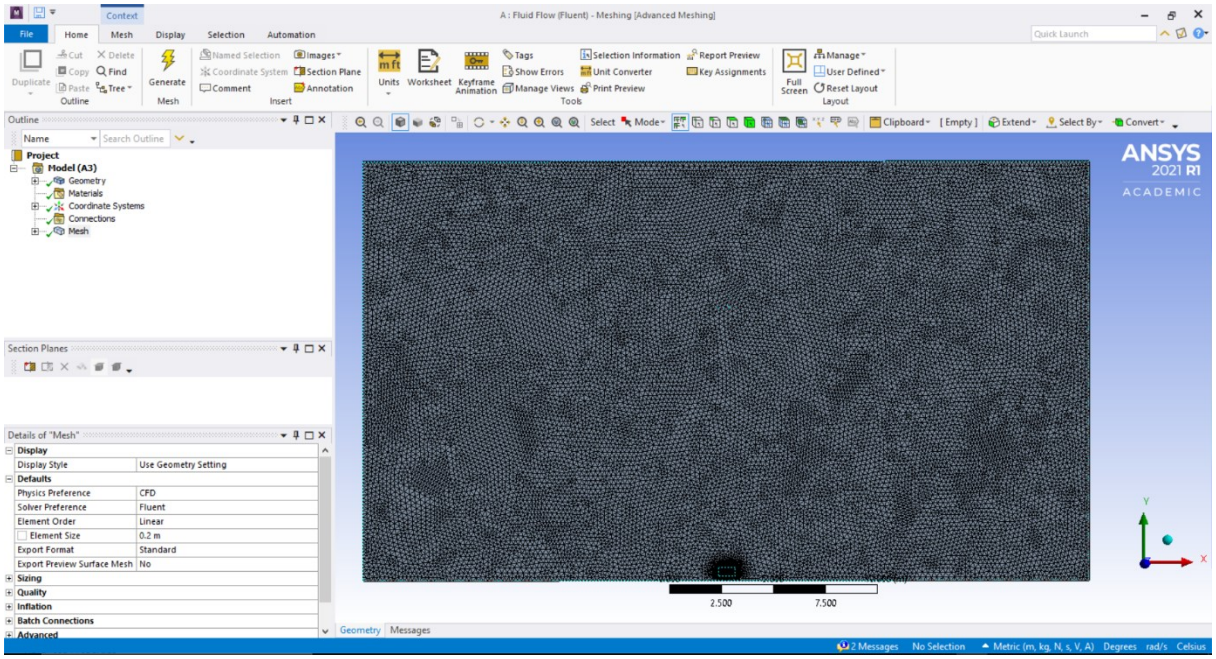

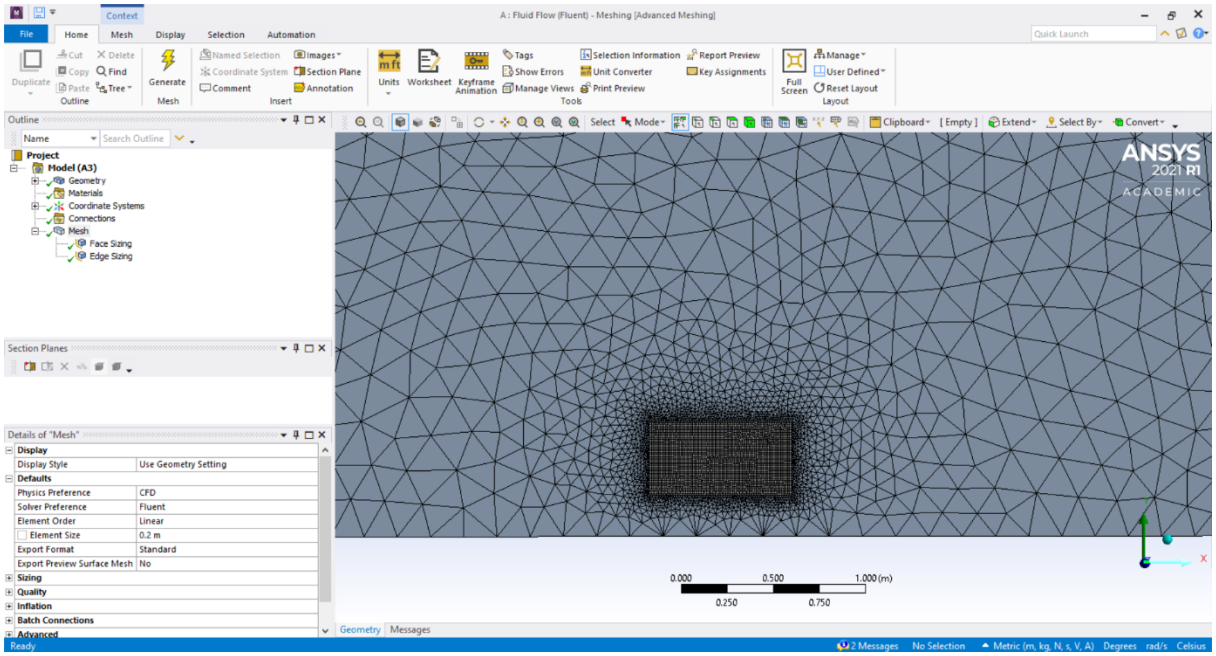

Mesh: Small-scale CGH2 tank (Transversal axis)

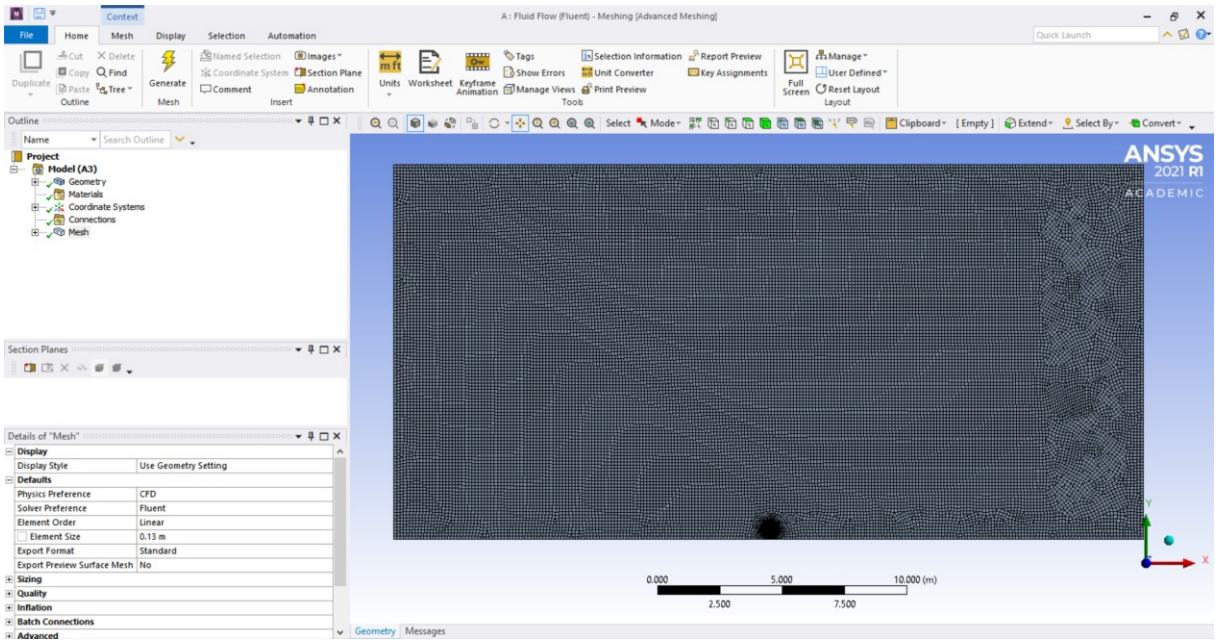

Mesh: Large-scale CGH2 tank (Longitudinal axis)

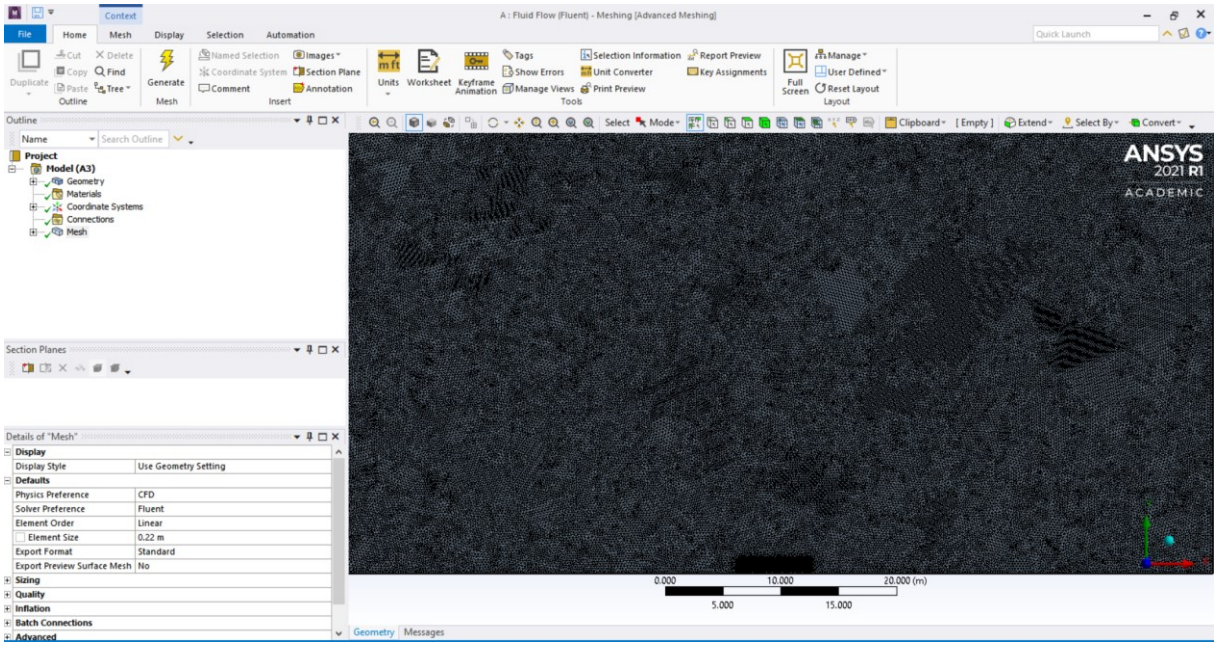

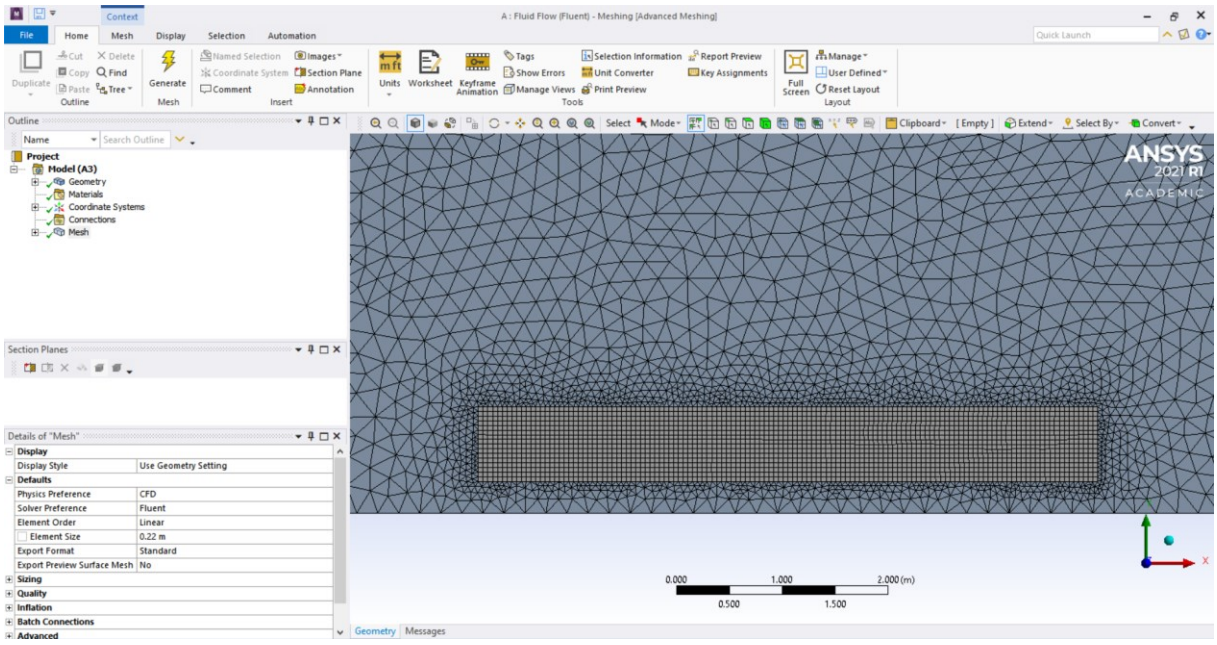

Mesh: Large-scale CGH2 tank (Transversal axis)

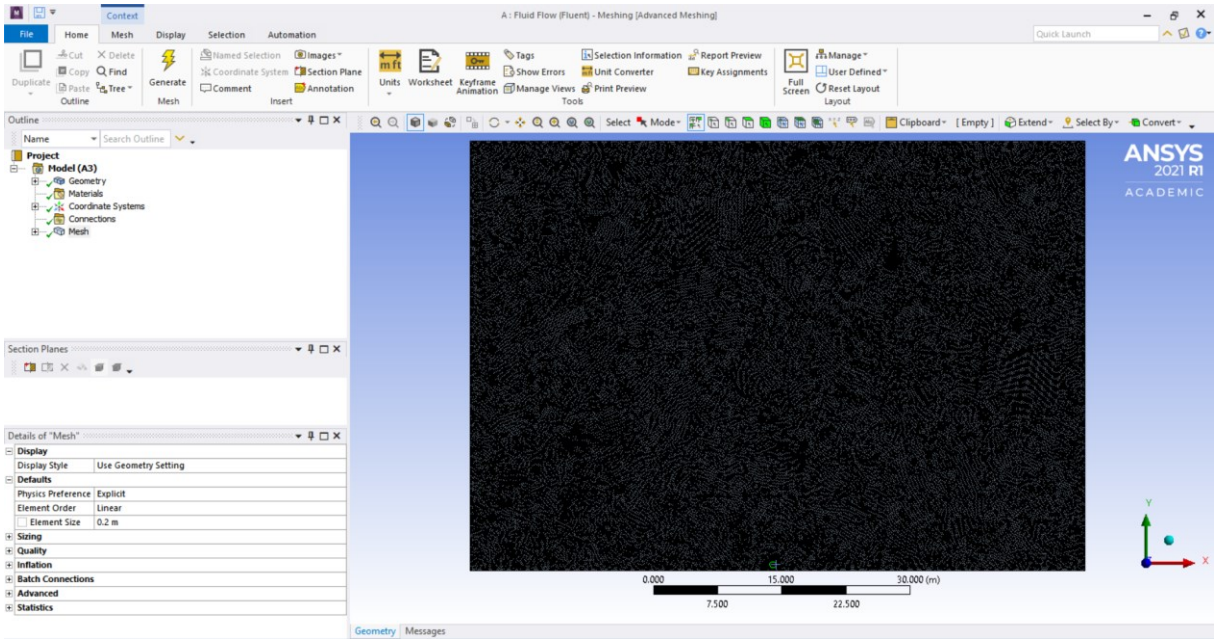

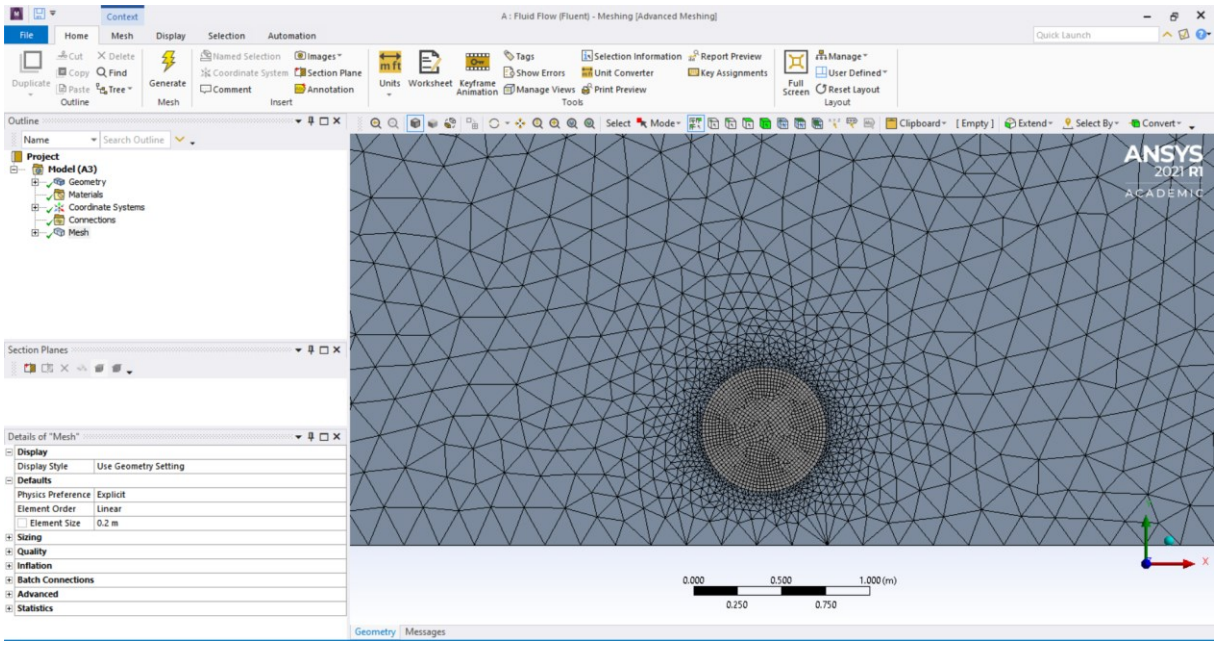
A : Fluid Flow (Fluent) - Meshing [Advanced Meshing]
File
Home
Mesh
Display
Selection
Automation
Outline
Project
Model (A3)
Geometry
Materials
Coordinate Systems
Connections
Mesh
Section Planes
Details of "Mesh"
Display
Display Style
Use Geometry Setting
Defaults
Physics Preference
Explicit
Element Order
Linear
Element Size
0.2 m
Sizing
Quality
Inflation
Batch Connections
Advanced
Statistics
ANSYS
2021 R1
ACADEMIC
0.000
0.500
1.000 (m)
0.250
0.750
Geometry
Messages

Appendix 2

Small-scale CGH2 tank

The yellow straight on the axis of cylinder to measure pressures on several distance points on this line.

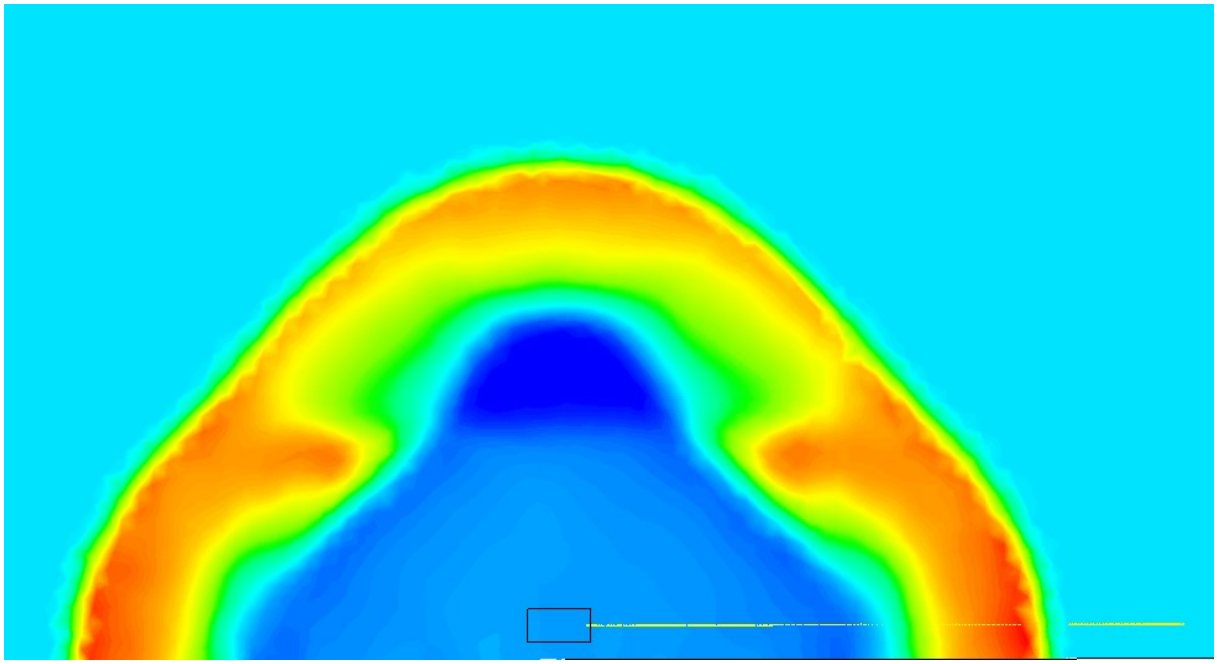

Large-scale CGH2 tank

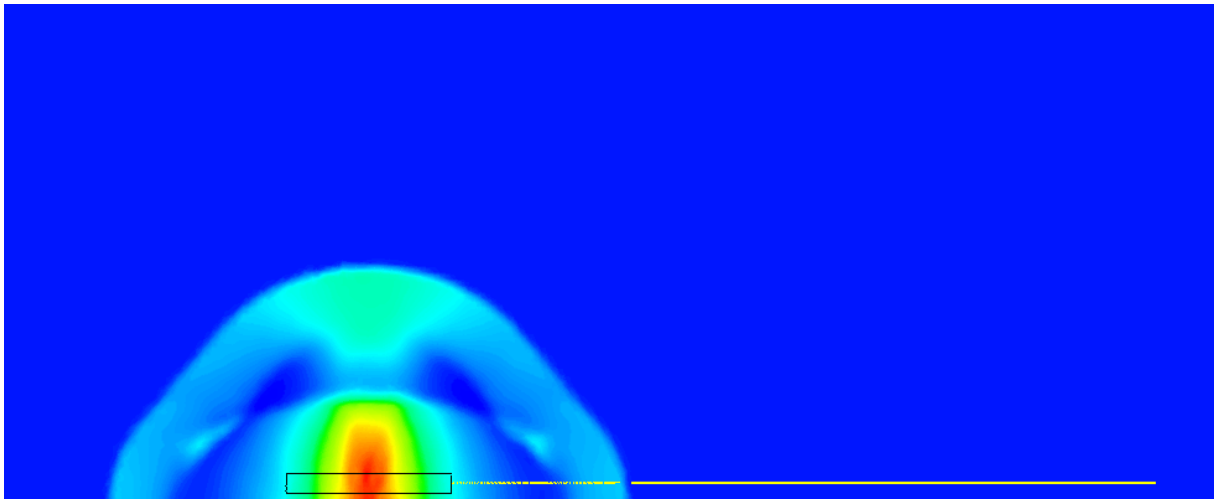

Appendix 3: Glossary of Terms

Cryogenics	Corresponding to temperatures less than 120 K
Deflagration	Deflagration is the propagation of a combustion zone at a velocity less than the speed of sound in the unreacted mixture.
Detonation	Detonation is the propagation of a combustion zone at a velocity greater than the speed of sound in the unreacted mixture.
Explosion	The sudden release of a large amount of energy generating a blast wave

NTNU

Norwegian University of
Science and Technology